FORSCHUNGSZENTRUM
ROSSENDORF e.V.

FZR

Archiv - Exemplar

FZR-114
November 1995

*Ulrich Grundmann*

# The Code DYN3DR for Steady-State and Transient Analyses of Light Water Reactor Cores with Cartesian Geometry

**Forschungszentrum Rossendorf** e.V.
**Postfach 51 01 19 · D-01314 Dresden**
**Bundesrepublik Deutschland**

**Telefon** **(0351) 260 3037**
**Telefax** **(0351) 260 2383**
**E-Mail** **grundman@fz-rossendorf.de**

# The Code DYN3DR for Steady-State and Transient Analyses of Light Water Reactor Cores with Cartesian Geometry

**U. Grundmann**

**November 1995**

**Forschungszentrum Rossendorf e. V.**
**Institut für Sicherheitsforschung**
Postfach 510119, D-01314 Dresden

The code DYN3D/M2 was developed for 3-dimensional steady-state and transient analyses of reactor cores with hexagonal fuel assemblies. The neutron kinetics of the new version DYN3DR is based on a nodal method for the solution of the 3-dimensional 2-group neutron diffusion equation for Cartesian geometry. The thermal-hydraulic model FLOCAL simulating the two phase flow of coolant and the fuel rod hehaviour is used in the two versions. The fundamentals for the solution of the neutron diffusion equations in DYN3DR are described. The 3-dimensional NEACRP benchmarks for rod ejections in LWR with quadratic fuel assemblies were calculated and the results were compared with the published solutions. The developed algorithm for neutron kinetics are suitable for using parallel processing. The behaviour of speed-up versus the number of processors is demonstrated for calculations of a static neutron flux distribution using a workstation with 4 processors.

**Zusammenfassung**

Der Code DYN3D/M2 wurde für 3-dimensionale stationäre und transiente Analysen von Reaktorkernen mit hexagonalen Brennelementen entwickelt. Die Neutronenkinetik der neuen Version DYN3DR basiert auf einer nodalen Methode zur Lösung der 3-dimensionlen 2-Gruppen-Neutronendiffusionsgleichung für kartesische Geometrie. Das thermohydraulische Modell FLOCAL zur Simulation der Zwei-Phasenströmung des Kühlmittels und des Brennstabverhaltens wird in beiden Versionen verwendet. Die Grundlagen zur Lösung der Neutronendiffusionsgleichungen in DYN3DR werden beschrieben. Die 3-dimensionalen NEACRP-Benchmarks für Regelstabauswürfe in LWR's mit quadratischen Brennelementen wurden berechnet und die Ergebnisse mit den veröffentlichten Lösungen verglichen. Der entwickelte Algorithmus für die Neutronenkinetik ist für Parallelrechner geeignet. Das Verhalten des Speedup-Faktors in Abhängigkeit von der Anzahl der Prozessoren wird für die Berechnung einer stationären Neutronenflußverteilung auf einer 4-Prozessor Workstation gezeigt.

## Content

## 1. Introduction

The new version DYN3DR of the code DYN3D/M2 /1/, initially designed for hexagonal-z core analysis, has been developed for reactor cores with rectangular fuel assemblies. The neutronic part of the two code versions can be used for staedy-state and transient calculations of reactor cores. The neutron kinetics in both versions is based on the solution of the two group neutron diffusion equation by nodal methods being different for the hexagonal /2/ and rectangular geometry. The thermal-hydraulic module FLOCAL /3,4/ simulating the two phase flow of coolant and the fuel rod hehaviour is used in both versions.

The paper describes the fundamentals of the neutron kinetics of the rectangular option and demonstrates the high accuracy of the code by comparisons with rod ejection benchmarks for a PWR with rectangular fuel assemblies /8,9/.

All parts of the code are written in FORTRAN-77. Since neutron kinetics is very time consuming the developed algorithm's are suitable for using parallel processing. Special commands for utilizing the parallel capabilities on SUN workstations are included in the neutronic part of the code. The code is running on other computers too, because the parallelizing commands are interpreted as comments by usual compilers. The speedup of neutronic calculations is demonstrated for a steady state solution of diffusion equation.

## 2. Neutron Kinetic Model

The time-dependent neutron diffusion equations for a node n are used in the following form

$$\frac{1}{v_1^n}\frac{\partial \Phi_1^n(\mathbf{r},t)}{\partial t} + \nabla \mathbf{J}_1^n(\mathbf{r},t) + \Sigma_r^n(t)\Phi_1^n(\mathbf{r},t) = \frac{1}{k_{eff}} \sum_{g'=1}^{2} (1-\beta_{g'}^n)\nu\Sigma_{f,g'}^n(t)\Phi_{g'}^n(\mathbf{r},t) + \sum_{j=1}^{M} \lambda_j^n C_j^n(\mathbf{r},t)$$

$$\frac{1}{v_2^n}\frac{\partial \Phi_2^n(\mathbf{r},t)}{\partial t} + \nabla \mathbf{J}_2^n(\mathbf{r},t) + \Sigma_a^n(t)\Phi_2^n(\mathbf{r},t) = \Sigma_s^n(t)\Phi_1^n(\mathbf{r},t) \qquad (1)$$

$$\frac{dC_j^n(\mathbf{r},t)}{dt} = \frac{1}{k_{eff}} \sum_{g'=1}^{2} \beta_{g'j}^n \nu\Sigma_{f,g'}^n(t)\Phi_{g'}^n(\mathbf{r},t) - \lambda_j^n C_j^n(\mathbf{r},t) \qquad j=1,....,M$$

$$\beta_g^n = \sum_{j=1}^{M} \beta_{gj}^n$$

with Fick's law

$$J_g^n(\mathbf{r},t) = -D_g^n(t)\nabla\Phi_g^n(\mathbf{r},t) \qquad (2)$$

where

| | |
|---|---|
| $\Phi_g^n(\mathbf{r},t)$ : | neutron flux of energy group g |
| $\mathbf{J}_g^n(\mathbf{r},t)$ : | net current of neutrons of group g |
| $\Sigma_r^n(t), \Sigma_a^n(t), \Sigma_s^n(t)$ : | macroscopic removal, absorption and scattering cross sections |
| $\nu\Sigma_{f,g}^n(t)$ : | macroscopic fission cross section multiplied by the number of fission neutrons |
| $v_g^n$ : | mean group velocities of neutrons |
| $C_j^n(\mathbf{r},t)$ : | density of precursors of group j |
| $\beta_{gj}^n$ : | effective fractions of delayed neutrons of group j for a fission with an incident neutron of group g in the node n |
| $\lambda_j$ : | decay constant for precursors of group j |
| $M$ : | number of different precursor groups |
| $k_{eff}$ : | eigenvalue of stationary state |

The time integration over the step $\Delta t$ is performed by using an implicit difference scheme and an exponential transformation technique

$$\Phi_g^n(\mathbf{r},t') = \exp[\Omega^n(t'-t+\Delta t)]\Psi_g^n(\mathbf{r},t') \tag{3}$$

$$t-\Delta t \le t' \le t$$

That yields the following approximation for the time derivative of neutron flux in the equations of prompt neutrons

$$\frac{d\Phi_g^n(\mathbf{r},t)}{dt} \approx \frac{1}{\Delta t}[(1+\Omega^n\Delta t)\Phi_g^n(\mathbf{r},t) - \exp(\Omega^n\Delta t)\Phi_g^n(\mathbf{r},t-\Delta t)] \tag{4}$$

The exponent $\Omega^n$ of the next time step can be determined from the logarithmic changes of fluxes within $\Delta t$ by

$$\Omega^n = \frac{1}{\Delta t}\ln\frac{\sum_{g=1}^{2}\Phi_g^n(\mathbf{r},t)}{\sum_{g=1}^{2}\Phi_g^n(\mathbf{r},t-\Delta t)} \tag{5}$$

Integrating the equations for the precursors of delayed neutrons an exponential behaviour of neutron fluxes with exponent $\Omega^n$ within the time step $\Delta t$ is assumed

$$C_j^n(\mathbf{r},t) = C_j^n(\mathbf{r},t-\Delta t)\exp(-\lambda_j\Delta t) + \frac{1-\exp[-(\lambda_j+\Omega^n)\Delta t]}{\lambda_j+\Omega^n}\frac{1}{k_{eff}}\sum_{g'=1}^{2}\beta_{g'j}^n\nu\Sigma_{f,g'}^n(t)\Phi_{g'}^n(\mathbf{r},t) \tag{6}$$

By inserting the expressions for time derivative of neutron flux (4) and the precursor densities (6) into the diffusion equations (1) the following inhomogeneous equation system is obtained:

$$-\nabla D_1^n(t)\nabla\Phi_1^n(\mathbf{r},t)+\left[\Sigma_r^n(t)+\frac{1+\Omega^n\Delta t}{v_1^n\Delta t}\right]\Phi_1^n(\mathbf{r},t)=\frac{1}{k_{eff}}\sum_{g'=1}^{2}\left(1-\sum_{j=1}^{M}\beta_{g'j}^n\delta_j^n\right)\nu\Sigma_{fg'}^n(t)\Phi_{g'}^n(\mathbf{r},t)$$

$$+\sum_{j=1}^{M}\lambda_j^n C_j^n(\mathbf{r},t-\Delta t)\exp(-\lambda_i\Delta t)+\frac{e^{\Omega^n\Delta t}}{v_1\Delta t}\Phi_1^n(\mathbf{r},t-\Delta t) \qquad (7)$$

$$-\nabla D_2^n(t)\nabla\Phi_2^n(\mathbf{r},t)+\left[\Sigma_a^n(t)+\frac{1+\Omega^n\Delta t}{v_2^n\Delta t}\right]\Phi_2^n(\mathbf{r},t)=\Sigma_s^n(t)\Phi_1^n(\mathbf{r},t)+\frac{e^{\Omega^n\Delta t}}{v_2\Delta t}\Phi_2^n(\mathbf{r},t-\Delta t)$$

with

$$\delta_j^n=\frac{\Omega^n+\lambda_j\exp\left[-(\lambda_j+\Omega^n)\Delta t\right]}{\lambda_j+\Omega^n}$$

The equation system can be written for both energy groups in a simpler form

$$-\nabla D_g^n(t)\nabla\Phi_g^n(\mathbf{r},t)+\tilde{\Sigma}_g^n(t)\Phi_g^n(\mathbf{r},t)=S_g^n(\mathbf{r},t) \qquad (8)$$

with the source terms

$$S_1^n(\mathbf{r},t)=\frac{1}{k_{eff}}\sum_{g'=1}^{2}\left(1-\sum_{j=1}^{M}\beta_{g'j}^n\delta_j^n\right)\nu\Sigma_{fg'}^n(t)\Phi_{g'}^n(\mathbf{r},t)$$

$$+\sum_{j=1}^{M}\lambda_j^n C_j^n(\mathbf{r},t-\Delta t)\exp(-\lambda_i\Delta t)+\frac{e^{\Omega^n\Delta t}}{v_1\Delta t}\Phi_1^n(\mathbf{r},t-\Delta t) \qquad (9)$$

$$S_2^n(\mathbf{r},t)=\Sigma_s^n(t)\Phi_1^n(\mathbf{r},t)+\frac{e^{\Omega^n\Delta t}}{v_2\Delta t}\Phi_2^n(\mathbf{r},t-\Delta t)$$

and the modified cross sections

$$\tilde{\Sigma}_1^n(t)=\left[\Sigma_r^n(t)+\frac{1+\Omega^n\Delta t}{v_1^n\Delta t}\right]$$

$$\tilde{\Sigma}_2^n(t)=\left[\Sigma_a^n(t)+\frac{1+\Omega^n\Delta t}{v_2^n\Delta t}\right] \qquad (10)$$

The term representing the modified fission source in (9) is iterated in the outer iteration process. The time t appears as a parameter in the inhomogeneous equation system only.

For the solution of the stationary equation prompt and delayed neutrons are in equilibrium. Thus a homogeneous equation system is obtained, because the source term consists in the fission source for the first group and in the scattering source for the second group only. Like the iteration in the transient calculation a fission source iteration process is applied also for the solution of static equations.

The node n being a rectangular box of volume

$$V^n = a_x^n \cdot a_y^n \cdot a_z^n \tag{12}$$

is considered when the fluxes are calculated. The used method is similar to nodal methods for rectangular and hexagonal geometry published in /5,6,7/. The index n of the box is omitted in the following. The equations are written without the parameter t for simplification also. Integration over the transverse directions y and z provides a one-dimensional equation in x direction.

$$-D_g \frac{d^2\Phi_g(x)}{dx^2} + \tilde{\Sigma}_g \bar{\Phi}_g(x) = \bar{S}_g(x) - \bar{L}_g(x) \tag{13}$$

with

$$\bar{\Phi}_g(x) = \frac{1}{a_y}\frac{1}{a_z} \int_{-\frac{a_y}{2}}^{\frac{a_y}{2}} dy \int_{-\frac{a_z}{2}}^{\frac{a_z}{2}} dz \Phi_g(\mathbf{r})$$

$$\bar{S}_g(x) = \frac{1}{a_y}\frac{1}{a_z} \int_{-\frac{a_y}{2}}^{\frac{a_y}{2}} dy \int_{-\frac{a_z}{2}}^{\frac{a_z}{2}} dz S_g(\mathbf{r}) \tag{14}$$

with the transversal integrated leakage term

$$\bar{L}_g(x) = \frac{-D_g}{a_y a_z} \int_{-\frac{a_y}{2}}^{\frac{a_y}{2}} dy \int_{-\frac{a_z}{2}}^{\frac{a_z}{2}} dz \left( \frac{\partial^2 \Phi_g(\mathbf{r})}{\partial y^2} + \frac{\partial^2 \Phi_g(\mathbf{r})}{\partial z^2} \right) \tag{15}$$

In analogy the y - and z - directions are treated. The one-dimensional transverse-integrated neutron flux is expanded in polynomials up to the second order and exponential functions being solutions of the homogeneous part of equations. Previously, the space coordinate x is transformed by

$$x \rightarrow x/a_x \tag{16}$$

With

$$\begin{aligned} D_g &\rightarrow D_g/a_x \\ \tilde{\Sigma}_g &\rightarrow \tilde{\Sigma}_g \cdot a_x \\ \bar{S}_g &\rightarrow \bar{S}_g \cdot a_x \\ \bar{L}_g &\rightarrow \bar{L}_g \cdot a_x \end{aligned} \tag{17}$$

the one-dimensional equation (13) is dimensionsless. The flux expansion has the following form

$$\bar{\Phi}_g(x) = \sum_{i=0}^{2} c_{g,i} w_i(x) + a_{g,1} e^{\kappa_g x} + a_{g,2} e^{-\kappa_g x} \tag{18}$$

with the polynomials

$$\begin{aligned} w_0(x) &= 1 \\ w_1(x) &= 2\sqrt{3}\, x \\ w_2(x) &= \sqrt{5}\left(\tfrac{1}{2} - 6x^2\right) \end{aligned} \tag{19}$$

satisfying the relations

$$\int_{-\frac{1}{2}}^{\frac{1}{2}} dx \cdot w_i(x) \cdot w_j(x) = \delta ij \tag{20}$$

$\delta_{ij}$ is Kronecker's symbol. The exponent $\kappa_g$ is obtained from the homogeneous part of equation (13) by

$$\kappa_g = \frac{\bar{\Sigma}_g}{D_g} \tag{21}$$

Assuming that the source terms $\bar{S}_g(x)$ in equation (13) show a more smooth behaviour in the box the source is expanded in the polynomials only.

$$\bar{S}_g(x) \approx \sum_{i=0}^{2} s_{g,i} w_i(x) \tag{22}$$

The transversal leakage $\bar{L}_g(x)$ is approximated in the same way from the current of the box and the adjacent boxes.

$$\bar{L}_g(x) \approx \sum_{i=0}^{2} l_{g,i} w_i(x) \tag{23}$$

Inserting these expansions into the equation (13) and using the boundary conditions, for example the incoming partial currents at the outer surfaces of the boxes, yield the coefficients of flux expansion (18). Before the next box is calculated the outgoing partial currents are determined. The other directions are treated in an analogous way. After finishing the inner iteration, a new fission source is calculated by updating the polynomial coefficients of fluxes. The outer iteration is accelerated by a Chebychev extrapolation scheme.

The nodal powers calculated by means of the nodal fluxes are transferred to the FLOCAL code. The updated values of fuel temperatures, coolant temperatures and coolant densities are used for the determination of cross sections. An iteration between neutron kinetics and thermal-hydraulics is carried out. Several kinetic steps $\Delta t_k$ are possible within one thermal hydraulic step $\Delta t_{th}$. The iterations over $\Delta t_{th}$ are finished, when convergence within preset limits is reached.

## 3. Results of Benchmark Calculations

In order to assess the different codes developed for transient analysis of reactor cores the so-called NEACRP benchmarks were defined /8/. The PWR problems were calculated by DYN3DR and the obtained results were compared with the published reference solutions /9/. The thermal-hydraulic model for the transient calculations in /10/ was specified similar to the NEACRP benchmarks in /8/. The version of FLOCAL slightly modified for the calculations in /10/ is also used here.

The problems A1, A2, B1, B2, C1 and C2 consist in rod ejections of central or peripheral rods at hot zero power (HZP) and full power (FP) conditions.

Short description of the 6 cases:

**A1**: Ejection of the central rod at HZP

**A2**: Ejection of the central rod at FP

**B1**: Ejection of a peripheral rod in octant geometry at HZP

**B2**: Ejection of a peripheral rod in octant geometry at FP

**C1**: Ejection of one peripheral rod at HZP

**C2**: Ejection of one peripheral rod at FP

The nominal power of the reactor is 2775 MW. There are 157 fuel assemblies and 64 reflector elements each with a side length of 20 cm in the core (see fig. 3.1). The core including the axial reflector is divided into 18 layers of different heights as given in the specifications of the problems /8/. The part of a fuel element in a layer is described by one node. In all cases the ejection time of rods is 0.1 s. The comparisons of DYN3DR with other codes and the reference solution for some parameters can be seen in tables 3.1 - 3.9. The given results of the other codes published in /9/ show the range of results. The tables contain the value of the published reference solutions and the deviations of the results obtained by the different codes. The reference solution was generated by the PANTHER code using 4 nodes per assembly in one layer. The generation of a mathematically exact reference solution is still open.

Table 3.1 shows the critical boron concentration of the initial steady states. The nodal power peaking factor of steady state solutions is listed in table 3.2. Table 3.3 gives the values for the static reactivity of the ejected rod. The positive reactivity insertions lead to an excursion of nuclear power reduced by the negative feedback. The results for the time of power peak and the power peak value can be seen in tables 3.4 and 3.5, respectively. The values of the power at the end of calculation ( $t = 5$ s ) are shown in table 3.6. The core averaged Doppler temperatures at $t = 5$ s are contained in table 3.7. The fuel centerline temperatures calculated with FLOCAL by an extrapolation using the average temperatures of the fuel layers are somewhat higher than the reference in all 6 cases (see table 3.8). The coolant exit temperatures are about 0.6 K higher than the reference values. The differences can be explained by the used procedure for water properties because the same deviations were obtained for the steady state of the FP

of the FP cases. The coolant exit temperatures and the deviations are listed in table 3.9 for the final calculation time.

Fig 3.A1.1 shows the power peak in the case A1 compared to the reference solution, fig 3.A1.2 displays the power curves up to t = 5 s. The behaviour of averaged Doppler temperature can be seen in fig 3.A1.3. The maximum fuel centerline temperature $T_{F,C}$ is depicted in figure 3.A1.4. The larger deviation seems to be caused by the mentioned extrapolation method. The same method was also applied for calculating the surface fuel temperature $T_{F,S}$. The Doppler temperature $T_D$ is given by

$$T_D = 0.3 \cdot T_{F,C} + 0.7 \cdot T_{F,S};$$

The figure 3.A1.5 shows the coolant exit temperatures, which are overestimated in DYN3DR in the static and transient results caused by the mentioned calculation of thermophysical properties. Similar notation is used for the curves of cases A2, B1, B2, C1, and C2. The most interesting cases C1 and C2 describing the ejection of a peripheral rod show significant changes of the radial flux shape. Fig. 3.C1.6 and 3.C2.6 show the asymmetric flux shape in axial layer 13 along the horizontal traverse (see fig 3.1) at the time of power maximum. A good agreement can be stated for the HZP case in fig. 3.C1.6. Fig. 3.C2.6 shows small deviations of about 5 % for the FP case in nodes near to the lower end of control rods.

As demonstrated by the tables, the results provided by DYN3DR are within the limits of the other codes. The time dependence of different quantities during the transient predicted by DYN3DR is close to the assumed reference solution in /9/.

## 4. Parallel Processing

First tests of the neutronic algorithm of DYN3DR were carried out by using the multiprocessor capabilities of a SUN-workstation SPARC 10/514 with a maximum of 4 processors. The code running on single processor machines could be translated by parallelizing compiler options without any changes of the source. That is possible since special commands for parallel DO-loops are interpreted as comments by other compilers.

Fig 4.1 shows the speedup of a 3 - dimensional steady state calculation in comparison to the theoretical curve. The algorithm gives identical results independent on the numbers of processors. The saving of CPU time for the static calculation is important for the parallelization of the transient calculation. The relatively small deviation to the theoretical curve in fig. 4.1 encourages to use a larger number of processors. The parallelization of the thermal-hydraulic code FLOCAL using parallel channel calculation is possible too.

## 5. Conclusions

The neutron kinetics of the rectangular code DYN3DR is briefly described. The results for the PWR rod ejection benchmarks are compared with the reference solution and published results of other codes. The good agreement with the reference solutions proves the code to be useful for transient calculations in PWR with rectangular fuel assemblies. The saving of CPU time by parallel processing is demonstrated for a steady state neutronic calculation. Further work on parallelization will be done for the transient neutronic calculation and the thermo-hydraulic code FLOCAL.

## References


/1/ Grundmann U.; Rohde, U.; "DYN3D/M2 - a Code for Calculation of Reactivity Transients in Cores with Hexagonal Geometry".
IAEA Technical Committee Meeting on Reactivity Initiated Accidents, Wien 1989
Report ZfK - 690, Rossendorf 1989
Report FZR 93 - 01,Rossendorf 1993

/2/ Grundmann, U.; " HEXNOD23 - A Two- and Three-Dimensional Nodal Code for Neutron Flux Calculation of Thermal Reactors with Hexagonal Geometry",
Report ZfK-557, Rossendorf, 1985

/3/ Rohde U; "Modelling of Fuel Rod Behaviour and Heat Transfer in the Code FLOCAL for Reactivity Accident Analysis Of Reactor Cores", 1st Baltic Heat Transfer Conference, Göteborg, 1991, published in "Transport Processes in Engineering 2: Recent Advances in Heat Transfer", Elsevier Publ., Amsterdam, 1992

/4/ Rohde U.; "Further Development of Modul FLOCAL for Thermo-hydraulic Calculation of Reactor cores in the version MOD 5",
Internal Report RPT-5/90, Rossendorf, 1990

/5/ Finnemann, H.; "Nodal Expansion Method for the Analysis of Space-Time Effects in LWR's", Proceedings of a "Specialists' Meeting on the Calculation of 3-Dimensional Rating Distributions in Operating Reactors",
Paris, 1979

/6/ Wagner, M. R.; "Three-Dimensional Nodal Diffusion and Transport Methods for Hexagonal Geometry"
Nucl. Sci. Engng **103,** p. 377-391 (1989)

/7/ Rajic H. L., Ougouag, A. M.; "ILLICO: A Nodal Neutron Diffusion Method for Modern Computer Architectures"
Nucl. Sci. Engng **103,** p. 392 (1989)

/8/ Finnemann, H.; Galati A.; "NEACRP 3-D LWR Core Transient Benchmark"
Report NEACRP-L-335, Rome, 1992

/9/ Finnemann H.; Bauer H.; Galati, A. Martinelli, R.; "Results of LWR Core Transient Benchmarks",
Report NEA/NSC/DOC(93) 25, OECD NEA, 1993

/10/ Knight, M. P.; Brohan, P.; Finnemann, H.; Huesken, J.; Grundmann, U.; Rohde, U.; "Comparison of Rod-Ejection Transient Calculations In Hexagonal-Z Geometry",
ANS Topical Meeting on Maths and Computations
Portland (USA), May 1995

## Tables

Table 3.1: LWR CORE TRANSIENT BENCHMARKS
PWR: Reference Value of Critical Boron Concentration and Deviations in (%)

| Case | A1 | A2 | B1 | B2 | C1 | C2 |
|---|---|---|---|---|---|---|
| Reference (ppm) | 567.70 | 1160.60 | 1254.60 | 1189.40 | 1135.30 | 1160.60 |
| OKAPI(s) | -1.215 | 0.974 | -0.375 | 0.572 | -0.484 | 0.974 |
| OKAPI(a) | -1.215 | 0.974 | -0.375 | 0.572 | -0.484 | 0.974 |
| BOREAS/TRAB | 23.71 | -0,250 | 0.486 | - 0.681 | 1.964 | -0.250 |
| CESAR | 3.576 | -2.292 | 0.988 | - 2.22 | 1.295 | -2.292 |
| PANBOX | -0.511 | 0.172 | -0.072 | 0.00 | -0.167 | 0.181 |
| QUABOX/CUBBOX | 0.458 | 0.327 | 1.124 | 0.336 | 1.092 | 0.310 |
| QUANDRY- EN | | | 0.510 | | 0.502 | |
| THYDE-NEU | | | | 5.936 | | |
| PRORIA | -41.695 | 3.739 | | | -0.467 | 4.170 |
| LWRSIM | 3.329 | 1.086 | 0.319 | 0.832 | 0.573 | 1.086 |
| SIMTRAN | 0.194 | 0.207 | 0.279 | 0.193 | 0.317 | 0.207 |
| ARROTTA | | | | | 0.326 | 5.032 |
| PANTHER | 0.740 | 0.698 | 0.558 | 0.504 | 0.590 | 0.698 |
| DYN3DR | 0.856 | 0.263 | 0.138 | 0.236 | 0.020 | 0.252 |

Table 3.2: LWR CORE TRANSIENT BENCHMARKS
PWR: Steady State Solution: Reference Value of Nodal Power Peaking Factor and Deviations (%)

| Case | A1 | A2 | B1 | B2 | C1 | C2 |
|---|---|---|---|---|---|---|
| Reference (abs.) | 2.874 | 2.221 | 1.932 | 2.109 | 2.187 | 2.221 |
| OKAPI(s) | 0.244 | 1.486 | -0.259 | 0.711 | -0.137 | 1.486 |
| OKAPI(a) | 0.244 | 1.486 | -0.259 | 0.711 | -0.137 | 1.486 |
| BOREAS/TRAB | 17.606 | 0.855 | 4.555 | -0.427 | 2.423 | 0.855 |
| CESAR | 8.559 | -1.846 | 8.178 | -2.323 | 13.397 | -1.846 |
| PANBOX | -0.974 | -0.630 | -0.259 | -0.759 | -0.137 | -0.675 |
| QUABOX/CUBBOX | -1.113 | -0.540 | 0.155 | -0.142 | 0.503 | -0.495 |
| QUANDRY- EN | | | -0.104 | | -0.137 | |
| LWRSIM | 4.175 | 1.891 | 3.621 | 0.806 | 3.978 | 1.891 |
| ARROTTA | | | | | -1.920 | 7.249 |
| PANTHER | -0.974 | -0.225 | -0.311 | -0.284 | -0.183 | -0.225 |
| DYN3DR | -0.574 | 0.090 | 0.430 | 0.474 | -0.274 | 0.135 |

Table 3.3: LWR CORE TRANSIENT BENCHMARKS
PWR: Reference Value of Reactivity Release and Deviations (%)

| Case | A1 | A2 | B1 | B2 | C1 | C2 |
|---|---|---|---|---|---|---|
| Reference (pcm) | 822.00 | 90.00 | 831.00 | 99.00 | 958.0 | 78.00 |
| CESAR | -4.015 | -4.444 | -2.407 | 8.081 | -1.983 | 2.564 |
| PANBOX | -1.460 | -1.111 | -0.963 | 2.020 | -0.731 | 2.564 |
| SIMTRAN | -1.460 | 0.000 | 0.000 | 2.020 | 0.313 | 3.846 |
| PANTHER | -1.825 | -3.333 | 0.120 | 1.010 | 0.731 | 1.282 |
| DYN3DR | -1.749 | -1.754 | 0.564 | -2.92 | -0.063 | 4.782 |

Table 3.4: LWR CORE TRANSIENT BENCHMARKS
PWR: Time of Power Maximum (Reference) and Deviations (%)

| Case | A1 | A2 | B1 | B2 | C1 | C2 |
|---|---|---|---|---|---|---|
| Reference (s) | 0.560 | 0.100 | 0.520 | 0.120 | 0.270 | 0.100 |
| OKAPI(s) | 5.357 | -20.000 | -3.846 | -16.667 | -11.111 | 0.000 |
| OKAPI(a) | 3.571 | | -7.692 | | -11.111 | |
| BOREAS/TRAB | 12.500 | 110.000 | -5.769 | 241.667 | 3.704 | 110.0 |
| CESAR | 37.500 | 0.000 | 17.308 | -16.667 | 11.111 | 0.000 |
| COCCINELLE | | | | | 18.519 | -20.0 |
| PANBOX | 7.143 | 0.000 | 0.000 | -8.333 | 0.000 | 0.000 |
| QUABOX/CUBBOX | 5.357 | -10.000 | -19.231 | -33.333 | 11.111 | -10.0 |
| QUANDRY- EN | | | -3.846 | | -3.704 | |
| REFLA/TRAC | -73.214 | | | | | |
| THYDE-NEU | | | | 575.000 | | |
| PRORIA | 221.490 | 0.000 | | | | 0.000 |
| SIMTRAN | 14.286 | 0.000 | 0.000 | -8.333 | 0.000 | 0.000 |
| ARROTTA | | | | | -3.704 | -20.0 |
| PANTHER | 16.071 | 0.000 | 0.000 | 0.000 | -3.704 | 20.0 |
| DYN3DR | 11.340 | 0.000 | -0.960 | -12.500 | -1.852 | -2.500 |

Table 3.5: LWR CORE TRANSIENT BENCHMARKS
PWR: Reference of Power Maximum (% of P/2775 MW) and Deviations (%)

| Case | A1 | A2 | B1 | B2 | C1 | C2 |
|---|---|---|---|---|---|---|
| Reference (%) | 117.900 | 108.000 | 244.100 | 106.300 | 477.300 | 107.100 |
| OKAPI(s) | -35.199 | -0.370 | 2.417 | -3.104 | -36.141 | -0.654 |
| OKAPI(a) | -0.339 | | 20.401 | | 30.170 | |
| BOREAS/TRAB | 25.106 | -0.185 | 3.154 | -0.188 | 164.215 | -0.093 |
| CESAR | -46.141 | 1.019 | -30.602 | 0.659 | -31.636 | 1.401 |
| COCCINELLE | | | | | -41.400 | -0.093 |
| PANBOX | -12.383 | 0.000 | -1.680 | 0.282 | -1.152 | 0.280 |
| QUABOX/CUBBOX | 12.299 | 0.833 | 125.604 | 1.035 | 130.254 | 1.774 |
| QUANDRY- EN | | | 0.901 | | 10.245 | |
| THYDE-NEU | | | | -0.188 | | |
| PRORIA | -73.028 | 0.278 | | | | 0.187 |
| SIMTRAN | -28.329 | 0.278 | -5.326 | 0.282 | -7.668 | 0.560 |
| ARROTTA | | | | | 3.394 | 0.934 |
| PANTHER | -23.749 | -0.278 | 8.193 | 0.094 | 16.740 | 0.093 |
| DYN3DR | -20.322 | 0.268 | 3.978 | -0.039 | -0.071 | -1.666 |

Table 3.6: LWR CORE TRANSIENT BENCHMARKS
PWR: Reference of Final Power (% of P/2775 MW) and Deviations (%)

| Case | A1 | A2 | B1 | B2 | C1 | C2 |
|---|---|---|---|---|---|---|
| Reference (%) | 19.600 | 103.500 | 32.000 | 103.800 | 14.600 | 103.000 |
| OKAPI(s) | -1.020 | -0.676 | -4.688 | -1.927 | 7.534 | -0.485 |
| OKAPI(a) | 25.000 | | 1.250 | | 47.260 | |
| BOREAS/TRAB | 70.408 | 0.773 | 12.500 | 0.674 | 191.096 | 0.874 |
| CESAR | -13.265 | -0.097 | -12.187 | 0.000 | -13.014 | 0.000 |
| COCCINELLE | | | | | 1.370 | 0.097 |
| PANBOX | 0.510 | 0.097 | 1.563 | 0.289 | 2.740 | 0.194 |
| QUABOX/CUBBOX | -0.510 | 0.676 | 3.750 | 0.771 | 4.110 | 1.068 |
| QUANDRY- EN | | | -23.438 | | -17.123 | |
| THYDE-NEU | | | | 0.963 | | |
| PRORIA | 26.020 | 0.193 | | | | 0.583 |
| SIMTRAN | 6.122 | 0.097 | 4.688 | 0.193 | 6.164 | 0.194 |
| ARROTTA | | | | | 19.178 | 0.000 |
| PANTHER | -0.510 | -0.097 | 1.563 | 0.096 | 2.740 | 0.097 |
| DYN3DR | 2.791 | 0.095 | 4.653 | 0.070 | 5.932 | 0.303 |

Table 3.7: LWR CORE TRANSIENT BENCHMARKS
Reference of Final Core Averaged Doppler Temperature and Deviations in (%)

| Case | A1 | A2 | B1 | B2 | C1 | C2 |
|---|---|---|---|---|---|---|
| Reference (°C) | 324.300 | 554.600 | 349.900 | 552.000 | 315.900 | 553.500 |
| OKAPI(s) | -0.278 | -0.252 | -0.343 | -0.707 | 0.380 | -0.199 |
| OKAPI(a) | 3.238 | | 0.800 | | 4.653 | |
| BOREAS/TRAB | 10.207 | 3.642 | 4.201 | 4.638 | 21.937 | 3.668 |
| CESAR | -0.648 | -7.339 | -0.657 | 6.902 | -0.443 | 7.371 |
| COCCINELLE | | | | | 0.222 | 0.452 |
| PANBOX | 0.463 | 1.100 | 0.915 | 1.159 | 0.538 | 1.102 |
| QUABOX/CUBBOX | | | 2.686 | 2.428 | | |
| QUANDRY- EN | | | 0.714 | | 0.823 | |
| THYDE-NEU | | | | 9.601 | | |
| PRORIA | 2.744 | 2.669 | | | | 3.847 |
| SIMTRAN | 1.079 | 2.164 | 1.600 | 2.174 | 0.950 | 2.186 |
| ARROTTA | | | | | -2.501 | -23.035 |
| PANTHER | -0.123 | -0.072 | 0.372 | -0.018 | 0.348 | -0.018 |
| DYN3DR | 0.469 | 0.315 | 1.294 | 0.264 | 0.681 | 0.275 |

Table 3.8: LWR CORE TRANSIENT BENCHMARKS
Reference of Maximum Fuel Centerline Temperature and Deviations (%)

| Case | A1 | A2 | B1 | B2 | C1 | C2 |
|---|---|---|---|---|---|---|
| Reference (°C) | 673.300 | 1691.800 | 559.800 | 1588.100 | 676.100 | 1733.500 |
| OKAPI(s) | -2.866 | -0.307 | -1.304 | -0.441 | -0.666 | -2.798 |
| OKAPI(a) | 19.768 | | 2.697 | | 33.279 | |
| CESAR | -6.728 | 0.254 | -5.359 | -0.252 | -2.721 | -0.329 |
| COCCINELLE | | | | | 1.834 | 3.340 |
| PANBOX | 0.965 | 0.106 | 1.536 | -0.025 | 2.588 | 0.317 |
| REFLA/TRAC | -0.624 | | 0.714 | | | |
| THYDE-NEU | | | | -0.617 | | |
| SIMTRAN | 3.802 | 1.170 | 3.019 | 0.686 | 5.118 | 1.546 |
| PANTHER | -1.233 | -0.136 | 0.875 | -0.164 | 3.062 | -0.012 |
| DYN3DR | 1.604 | 0.669 | 3.530 | 0.929 | 4.788 | 1.603 |

Table 3.9: LWR CORE TRANSIENT BENCHMARKS
Reference of Final Coolant Outlet Temperature and Deviations (%)

| Case | A1 | A2 | B1 | B2 | C1 | C2 |
|---|---|---|---|---|---|---|
| Reference ($^{o}$C) | 293.100 | 324.600 | 297.600 | 324.700 | 291.500 | 324.500 |
| OKAPI(s) | -0.102 | -0.031 | -0.134 | -0.154 | 0.069 | 0.000 |
| OKAPI(a) | 0.580 | | 0.101 | | 0.892 | |
| BOREAS/TRAB | 1.638 | 0.154 | 0.470 | 0.123 | 3.636 | 0.154 |
| CESAR | -0.307 | -0.031 | -0.437 | -0.031 | -0.206 | -0.031 |
| COCCINELLE | | | | | | |
| PANBOX | 0.034 | 0.154 | 0.101 | 0.154 | 0.069 | 0.154 |
| QUABOX/CUBBOX | -0.034 | 0.092 | 0.101 | 0.154 | -0.034 | 0.062 |
| QUANDRY- EN | | | -1.647 | | -0.755 | |
| THYDE-NEU | | | | 0.400 | | |
| | | | | | | |
| PRORIA | 0.068 | 1.078 | | | | -1.079 |
| SIMTRAN | 0.068 | -0.031 | 0.101 | -0.031 | 0.069 | -0.031 |
| ARROTTA | | | | | 0.343 | 0.000 |
| PANTHER | -0.034 | 0.031 | 0.067 | 0.031 | 0.069 | 0.031 |
| DYN3DR | 0.060 | -0.117 | 0.239 | 0.176 | 0.129 | 0.200 |

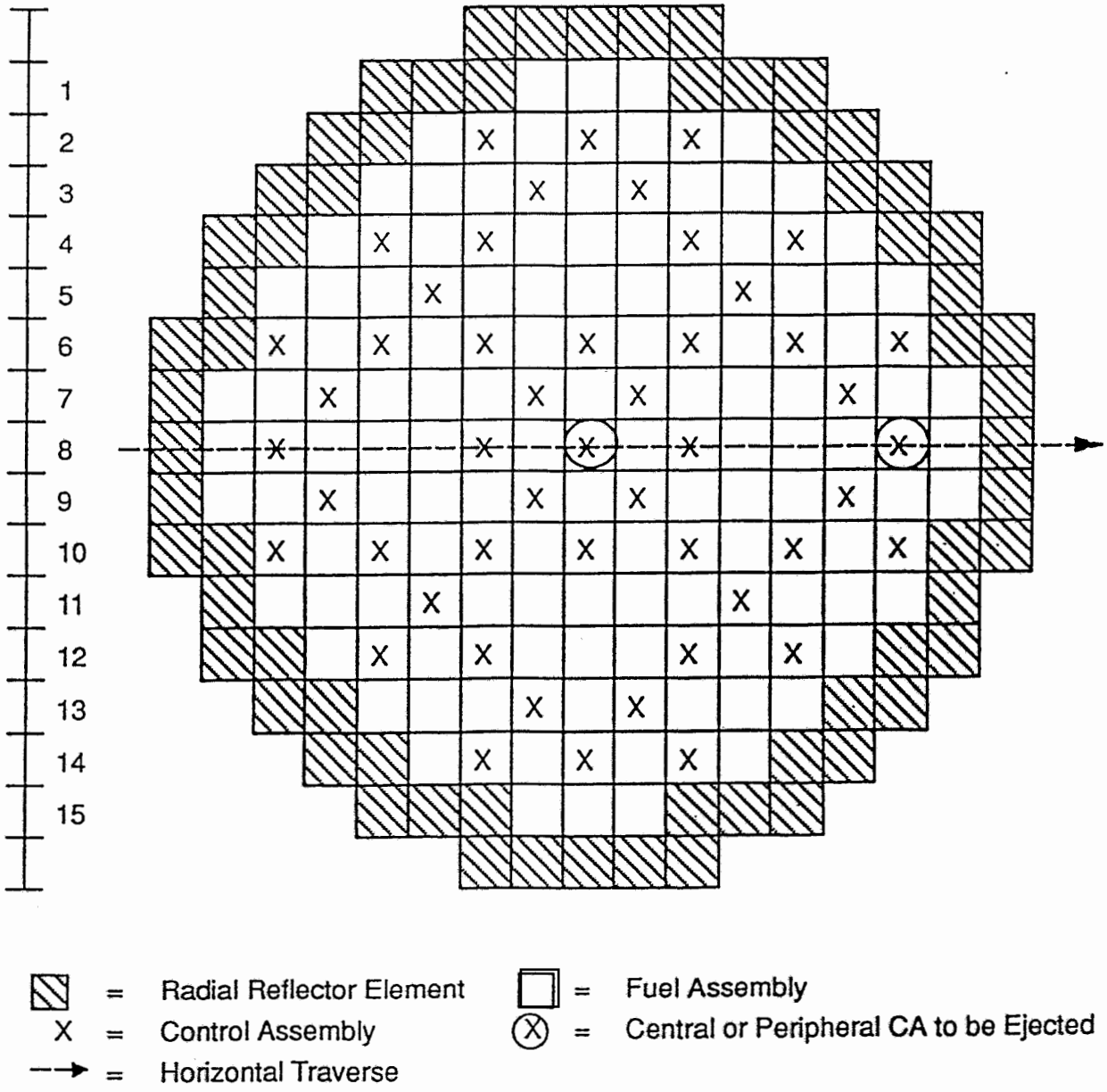


Fig. 3.1: Core Map of the PWR Benchmark Problems

PWR Case A1: Ejection of Central Rod at HZP

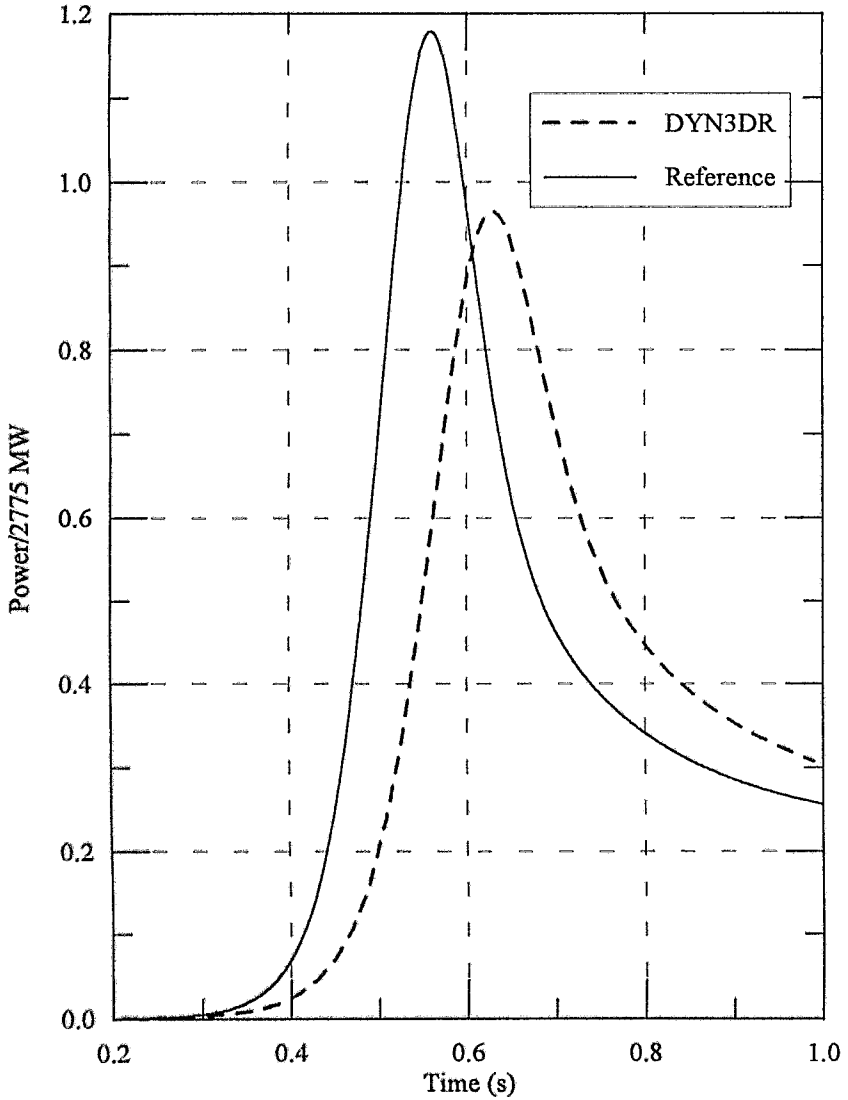


Fig. 3.A1.1: Nuclear Power

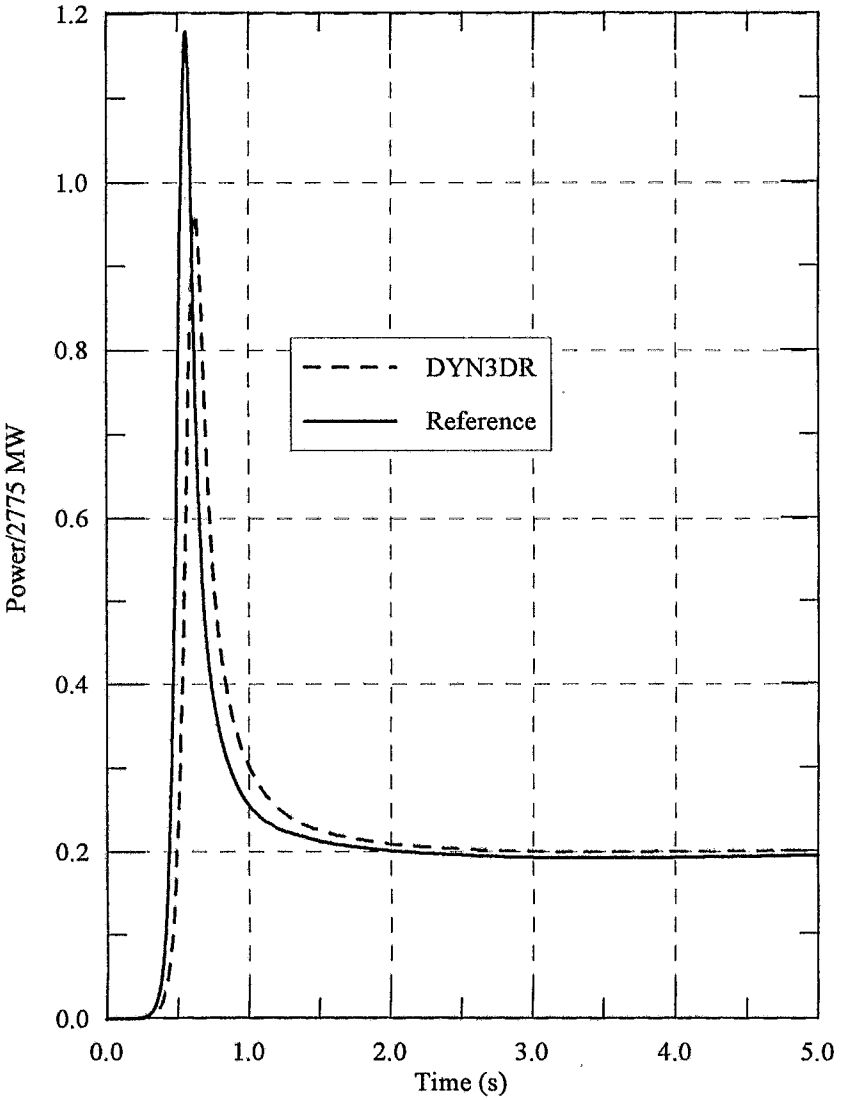


Fig. 3.A1.2: Nuclear Power

PWR Case A1: Ejection of Central Rod at HZP

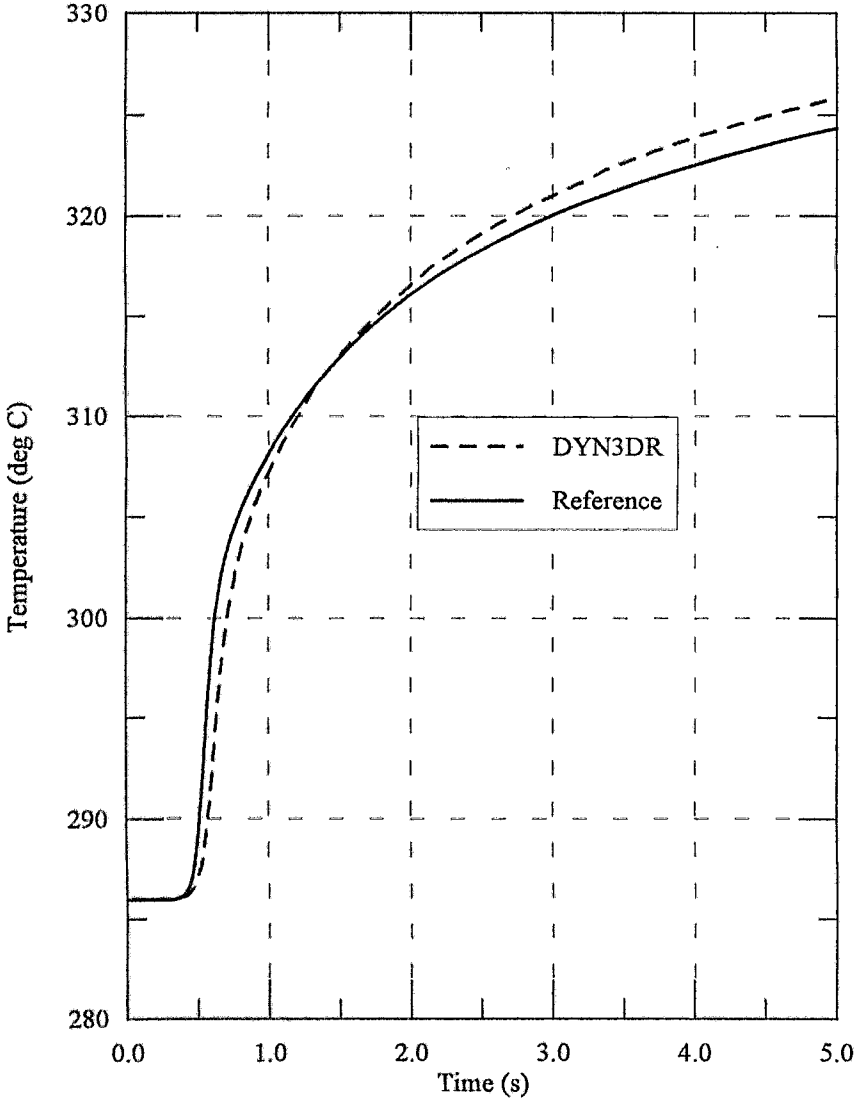


Fig. 3.A1.3: Core Averaged Doppler Temperature

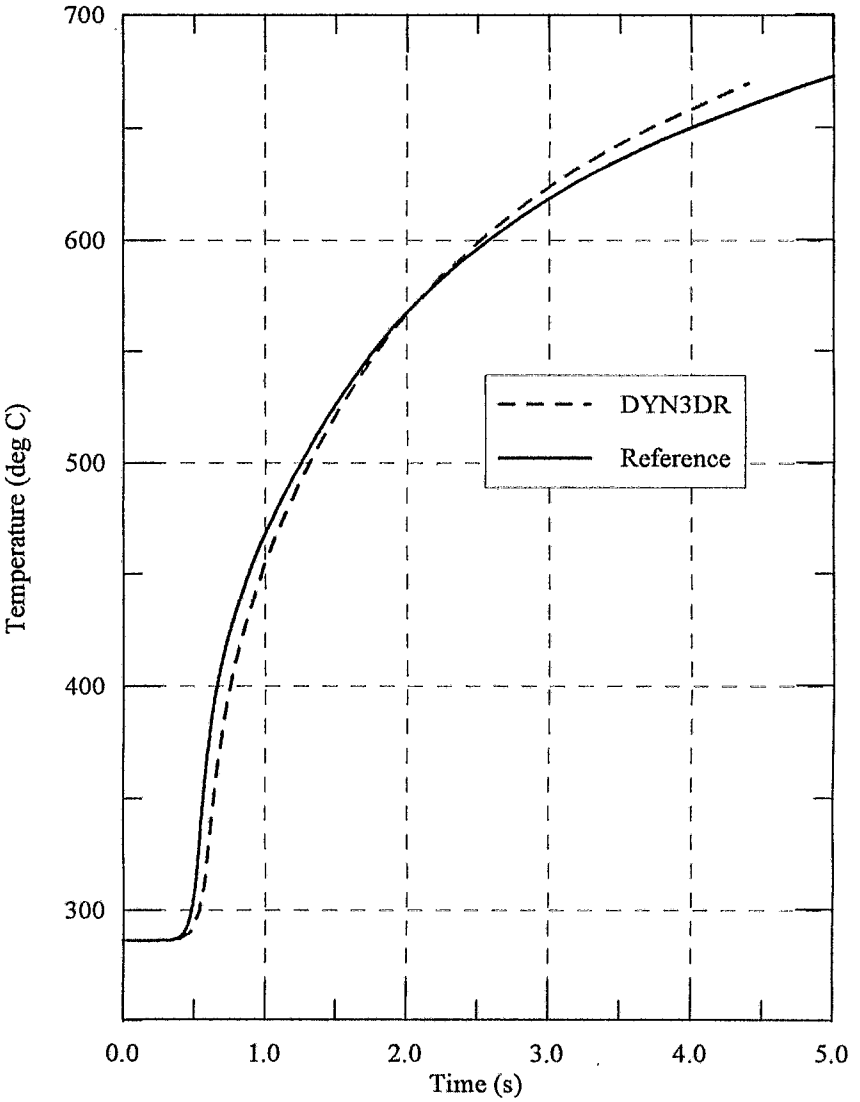


Fig. 3.A1.4: Maximum Fuel Centerline Temperature

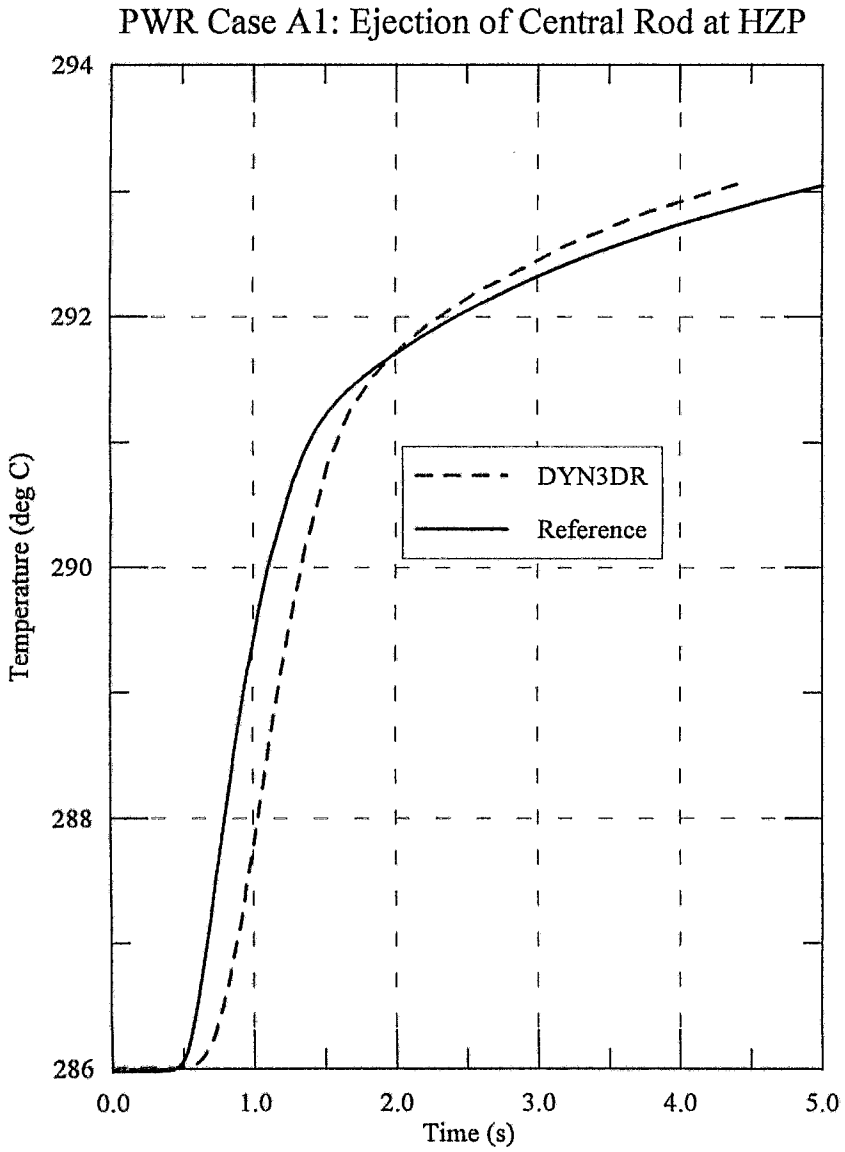


Fig. 3.A1.5: Coolant Exit Temperature

PWR Case A2: Ejection of Central Rod at FP

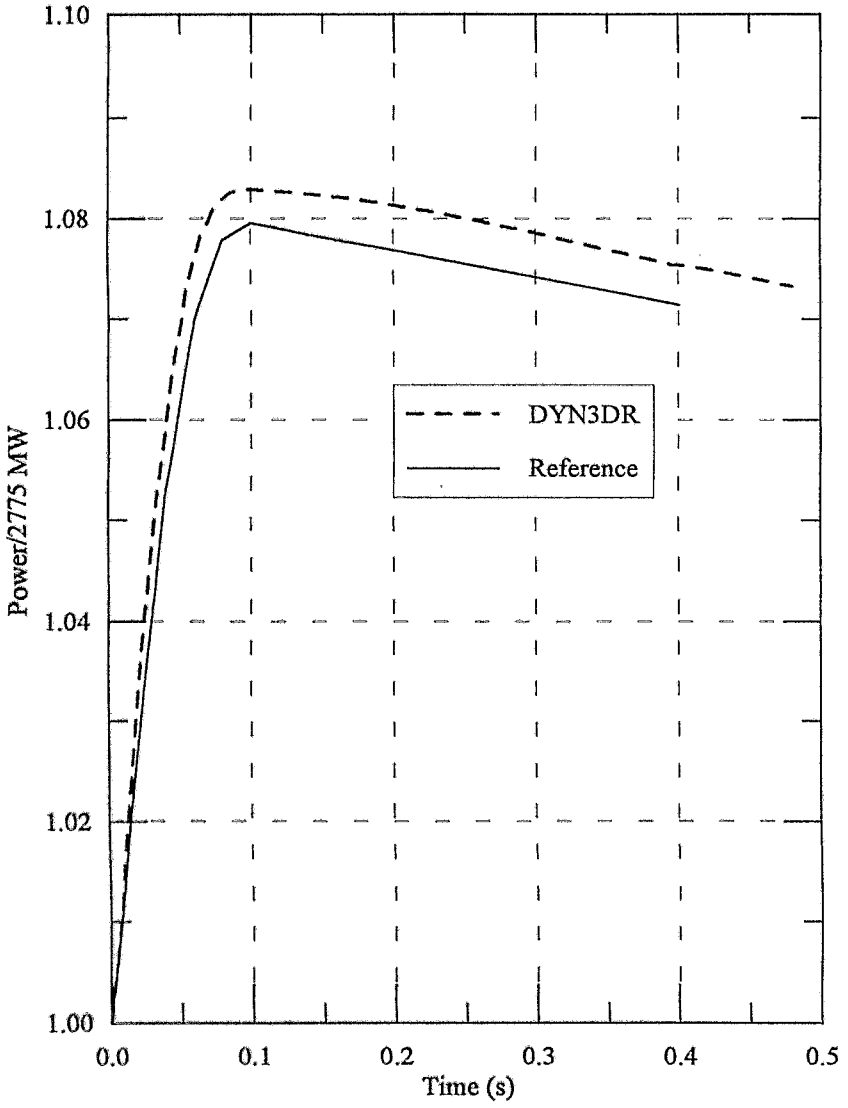


Fig. 3.A2.1: Nuclear Power

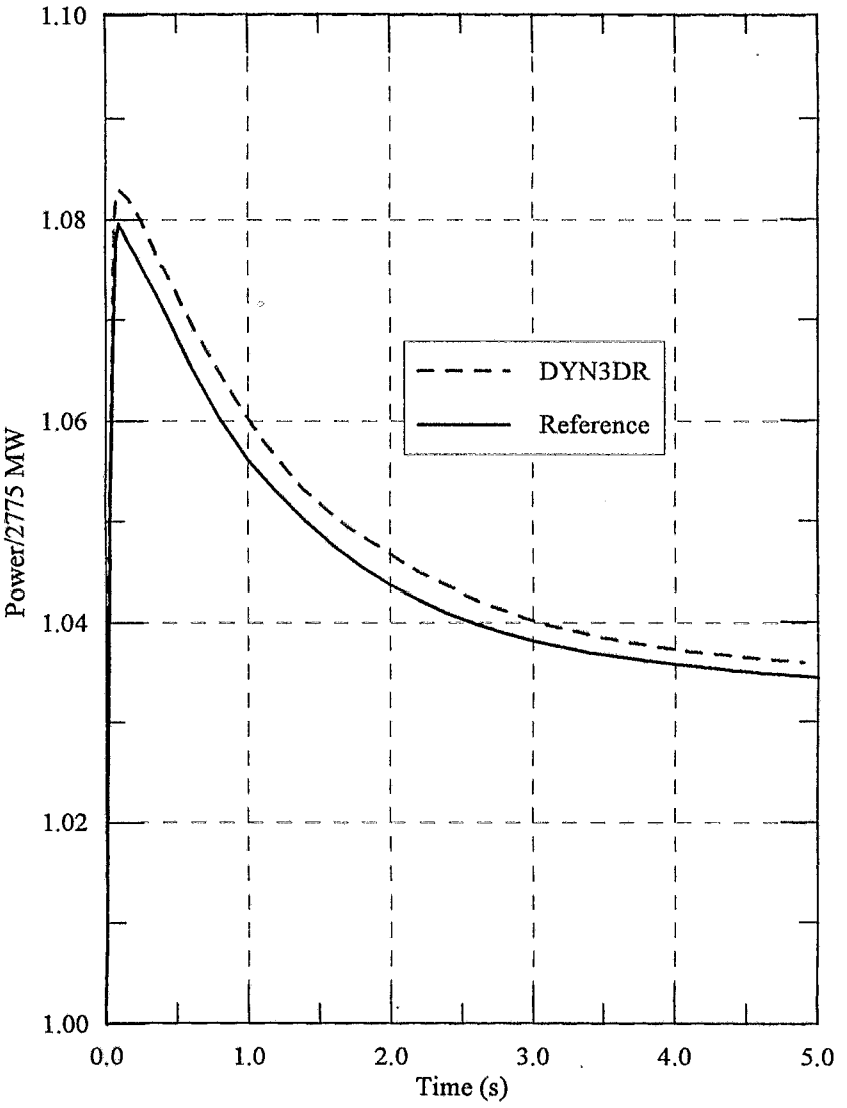


Fig. 3.A2.2: Nuclear Power

PWR Case A2: Ejection of Central Rod at FP

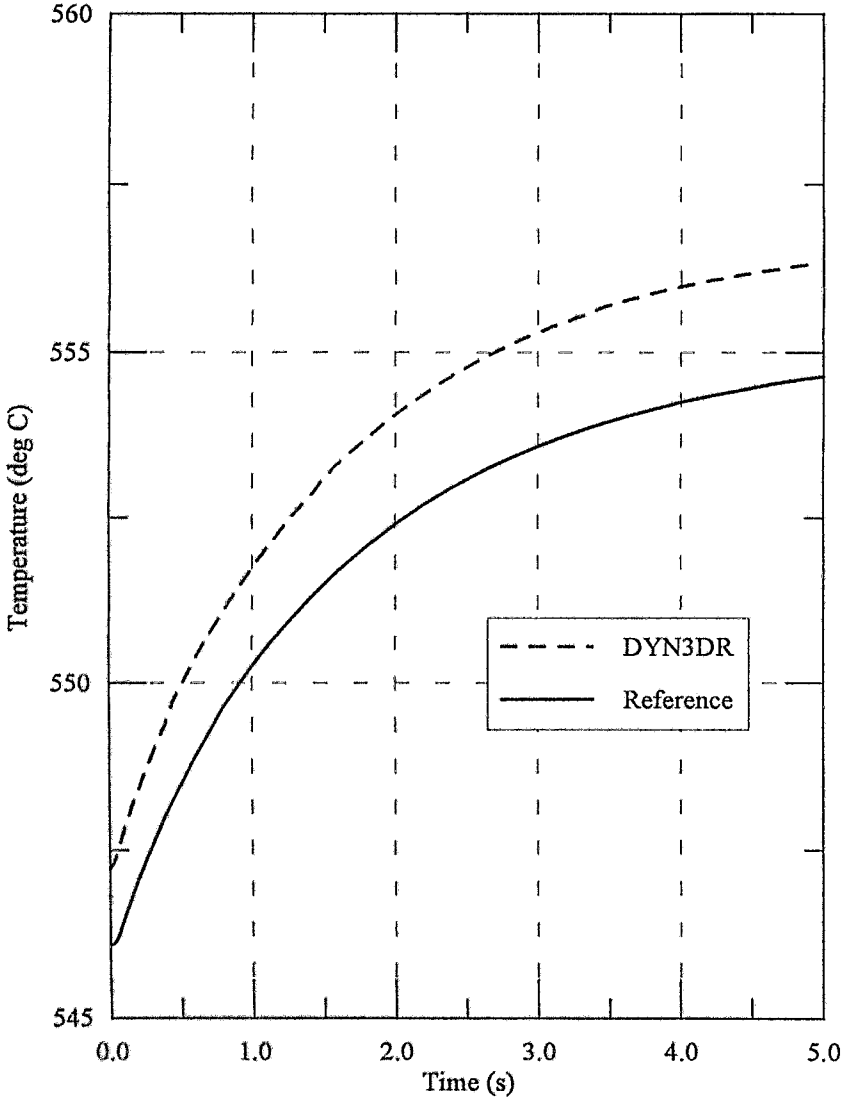


Fig. 3.A2.3: Core Averaged Doppler Temperature

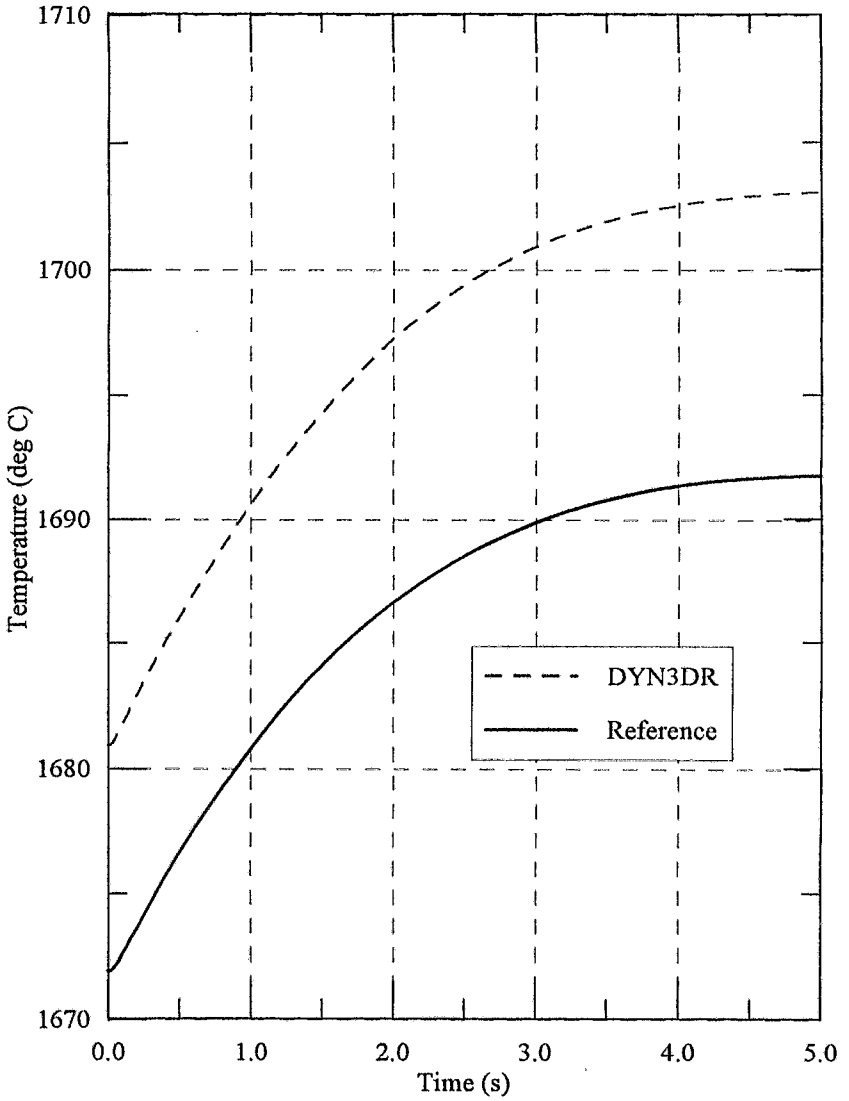


Fig. 3.A2.4: Maximum Fuel Centerline Temperature

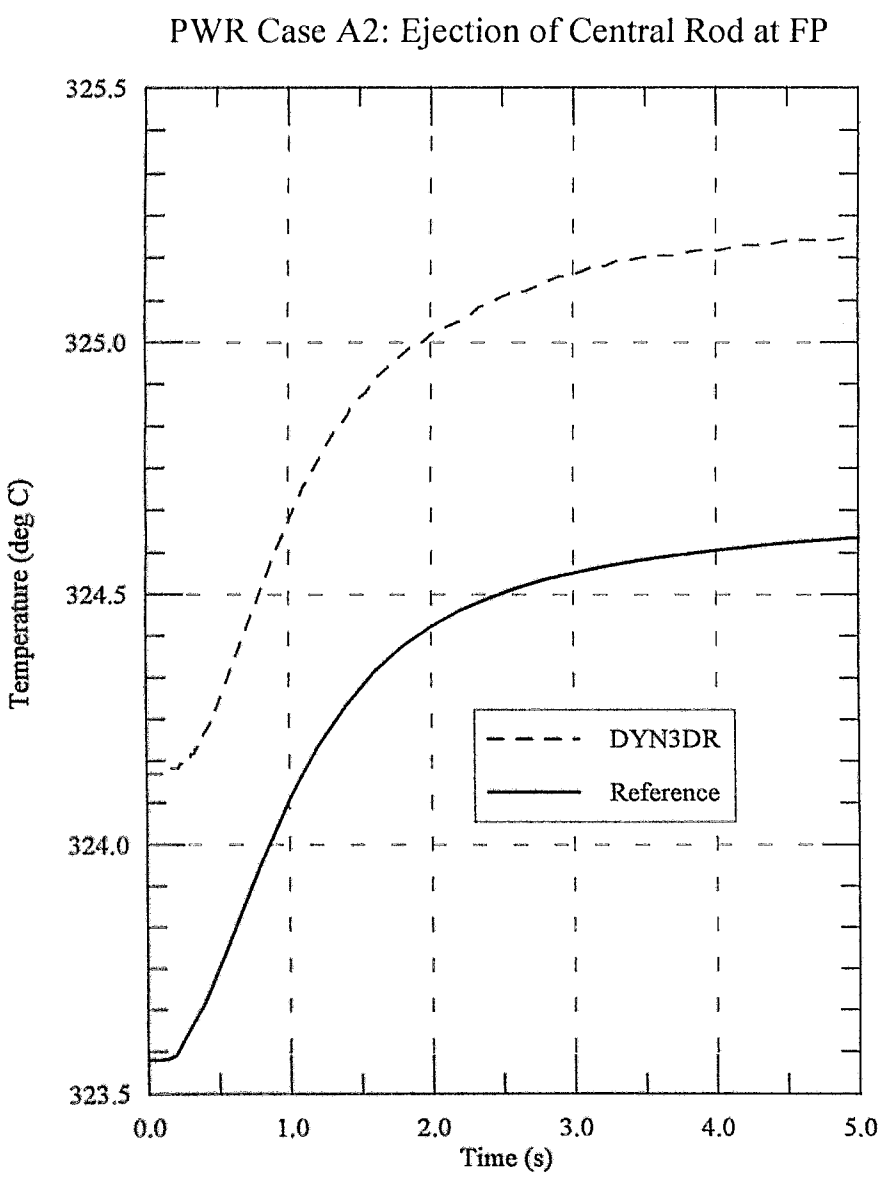


Fig. 3.A2.5: Coolant Exit Temperature

PWR Case B1: Ejection of a Peripheral Rod in Octant Geometry at HZP

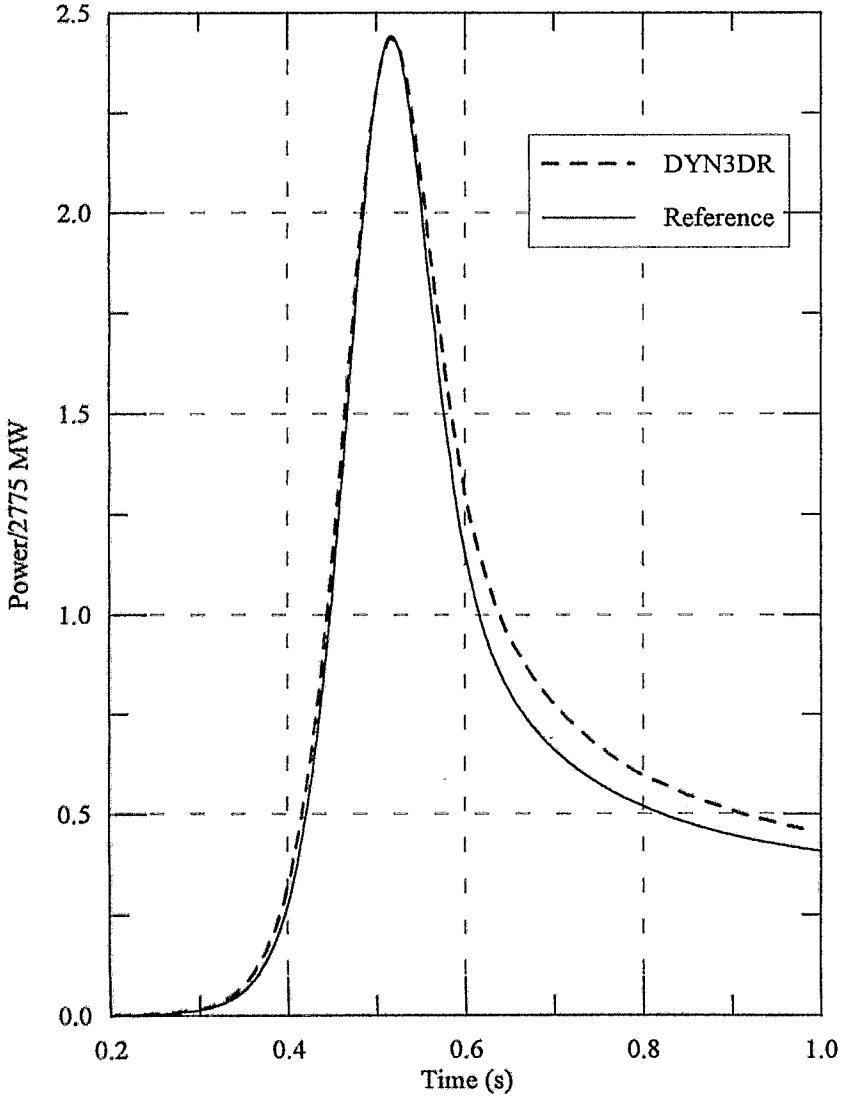


Fig. 3.B1.1: Nuclear Power

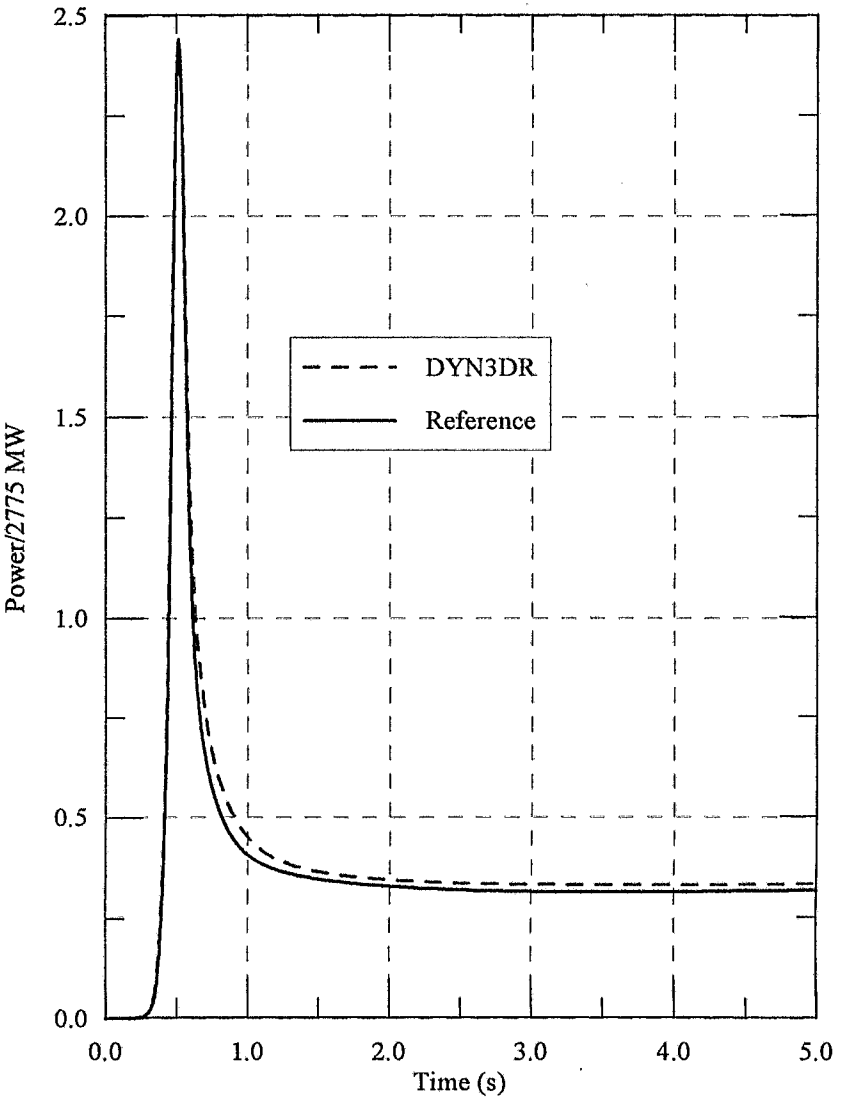


Fig. 3.B1.2: Nuclear Power

PWR Case B1: Ejection of a Peripheral Rod in Octant Geometry at HZP

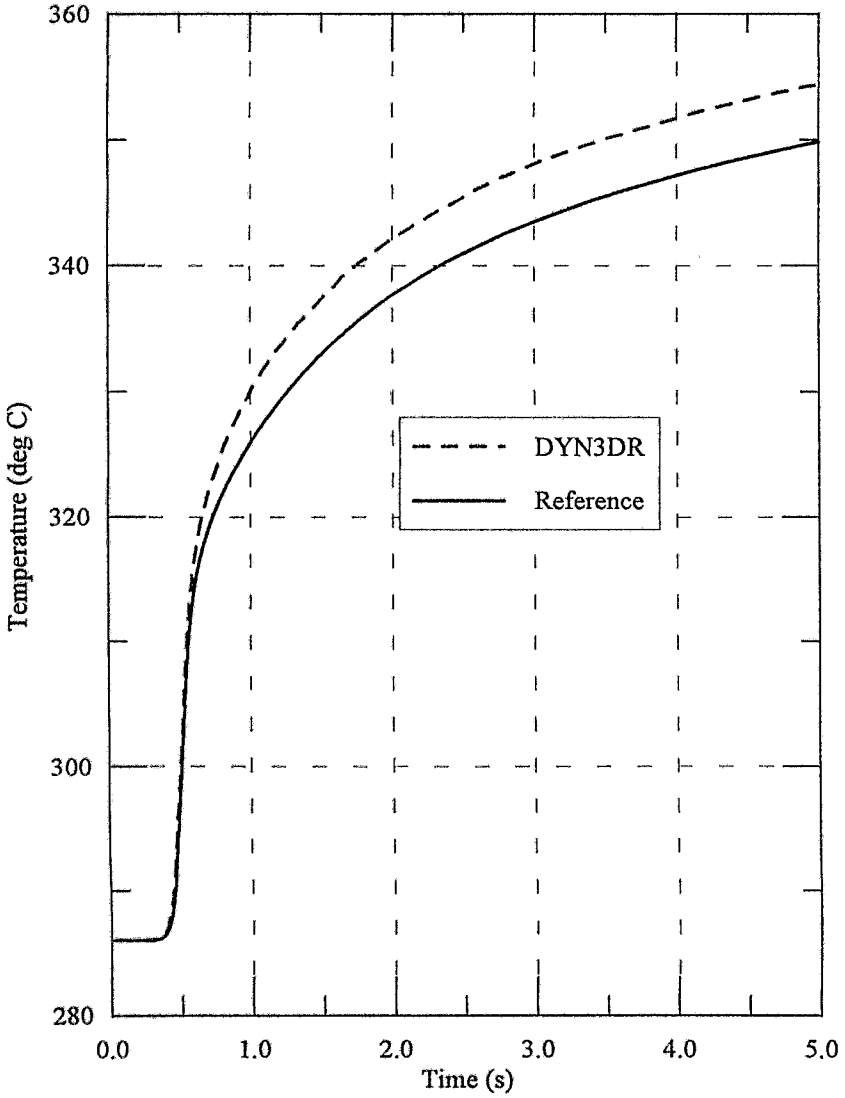


Fig. 3.B1.3: Core Averaged Doppler Temperature

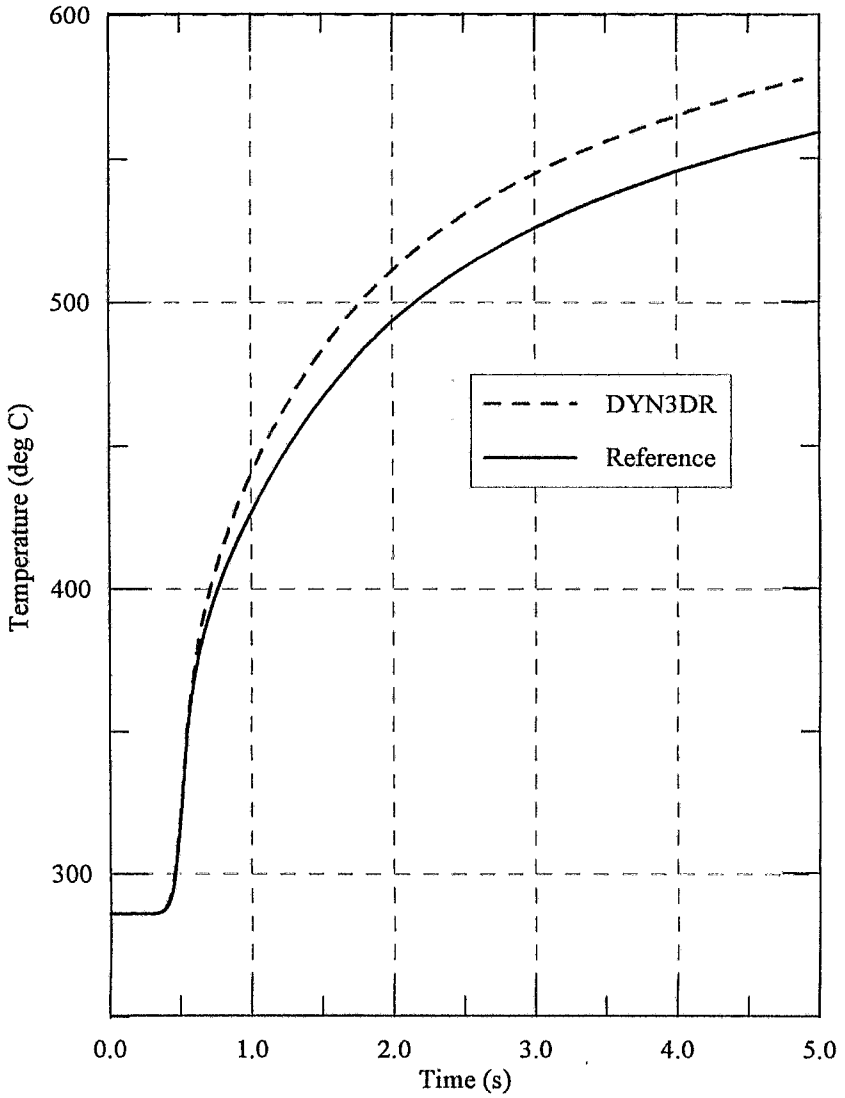


Fig. 3.B1.4: Maximum Fuel Centerline Temperature

PWR Case B1: Ejection of a Peripheral Rod in Octant Geometry at HZP

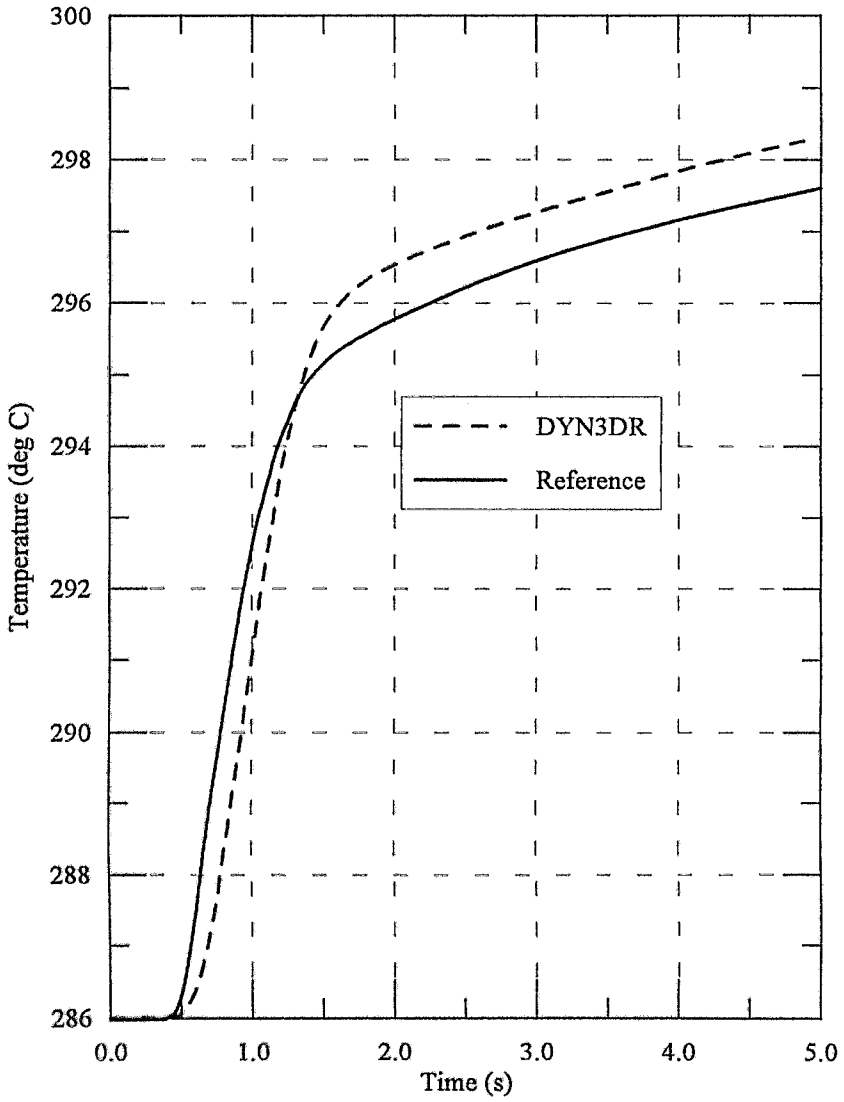


Fig. 3.B1.5: Coolant Exit Temperature

PWR Case B2: Ejection of a Peripheral Rod in Octant Geometry at FP

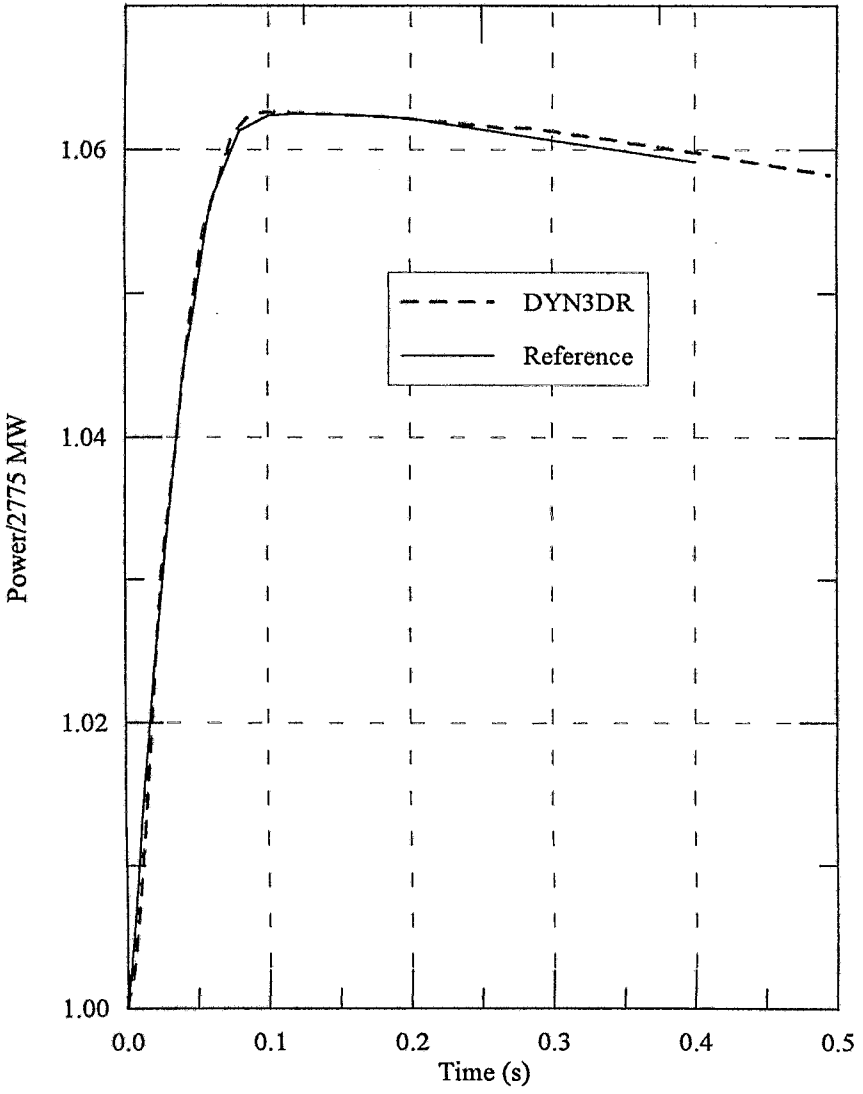


Fig. 3.B2.1: Nuclear Power

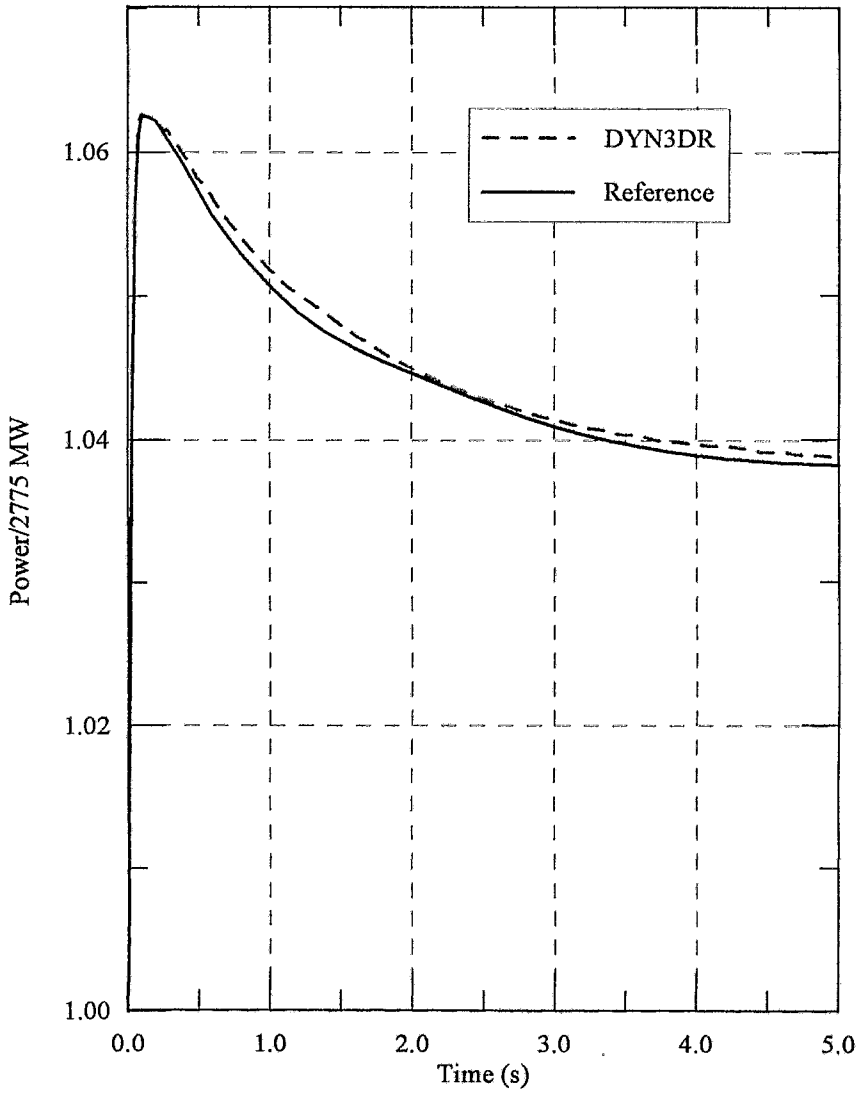


Fig. 3.B2.2: Nuclear Power

PWR Case B2: Ejection of a Peripheral Rod in Octant Geometry at FP

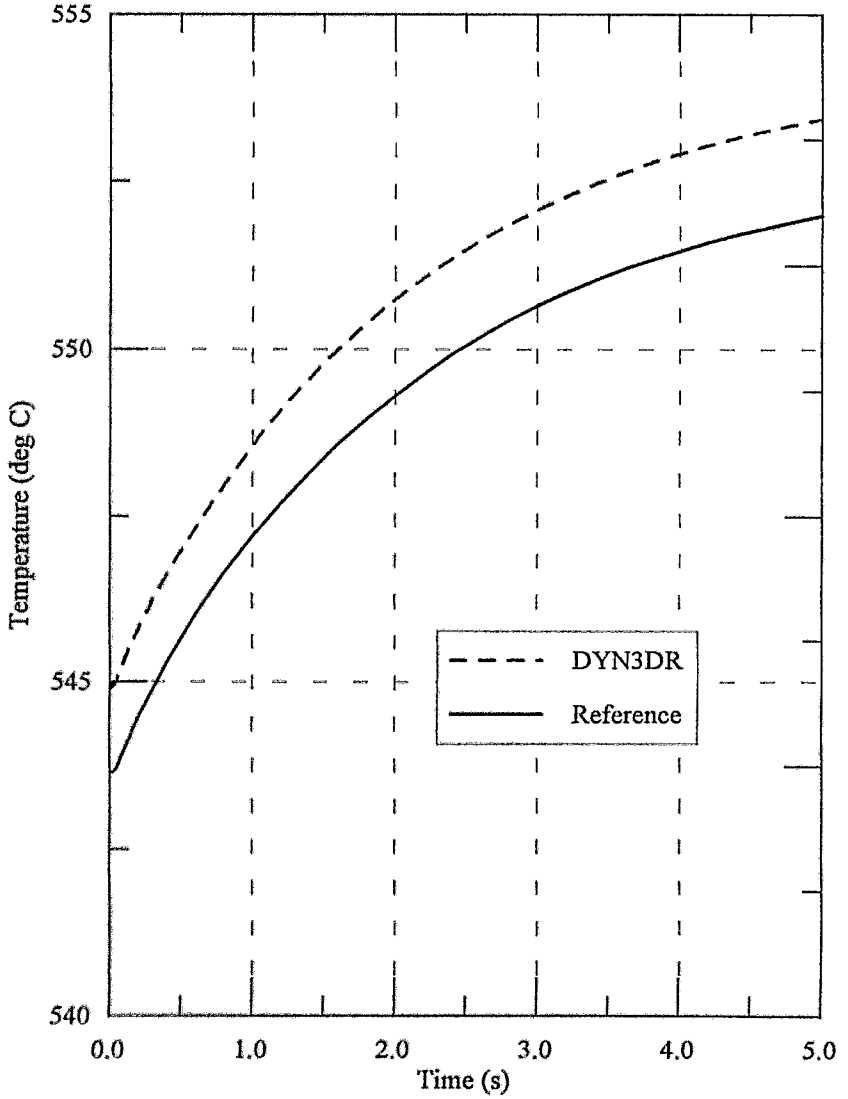


Fig. 3.B2.3: Core Averaged Doppler Temperature

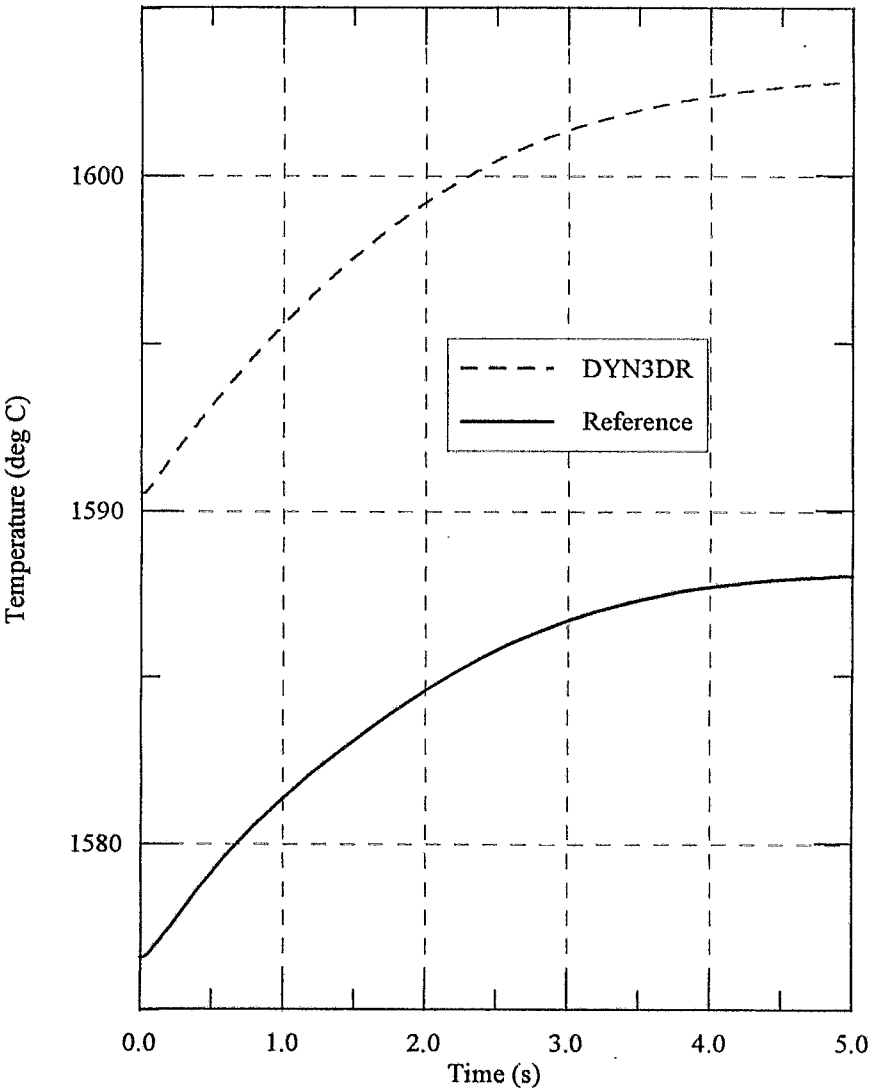


Fig. 3.B2.4: Maximum Fuel Centerline Temperature

PWR Case B2: Ejection of a Peripheral Rod in Octant Geometry at FP

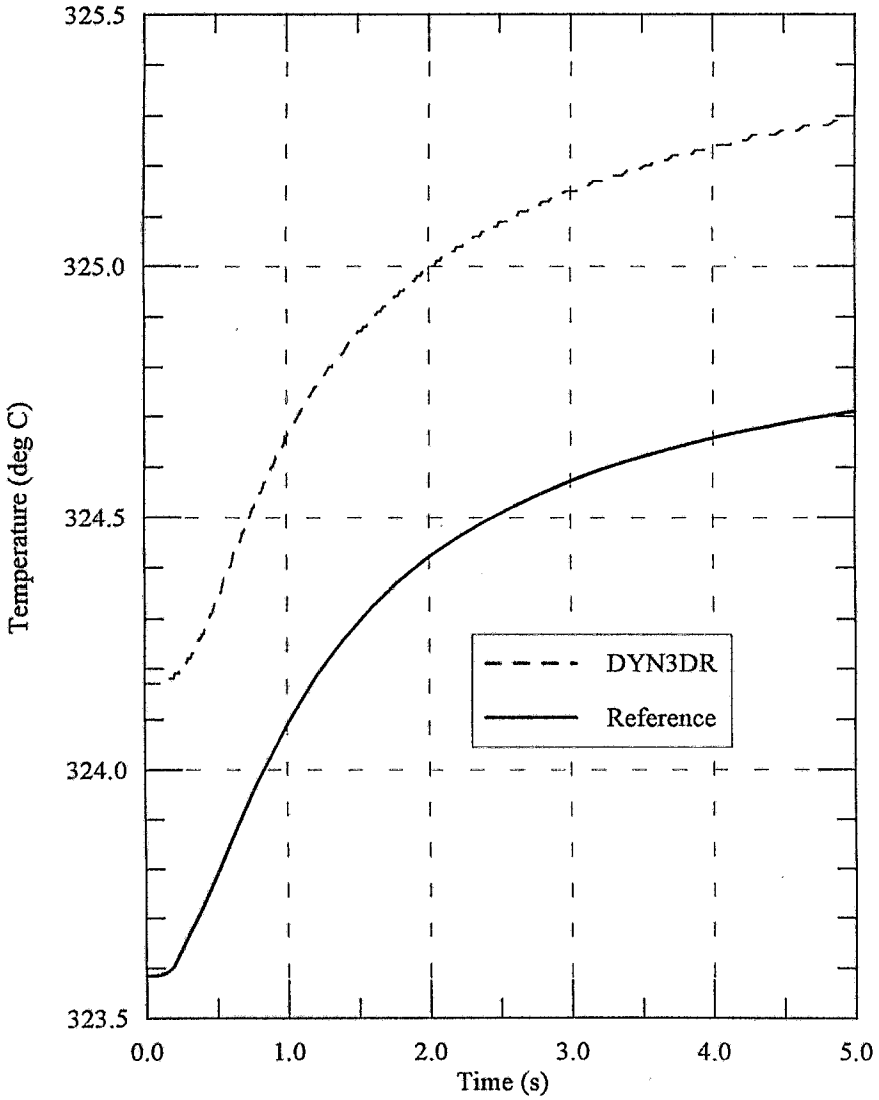


Fig. 3.B2.5: Coolant Exit Temperature

PWR Case C1: Ejection of a Peripheral Rod at HZP

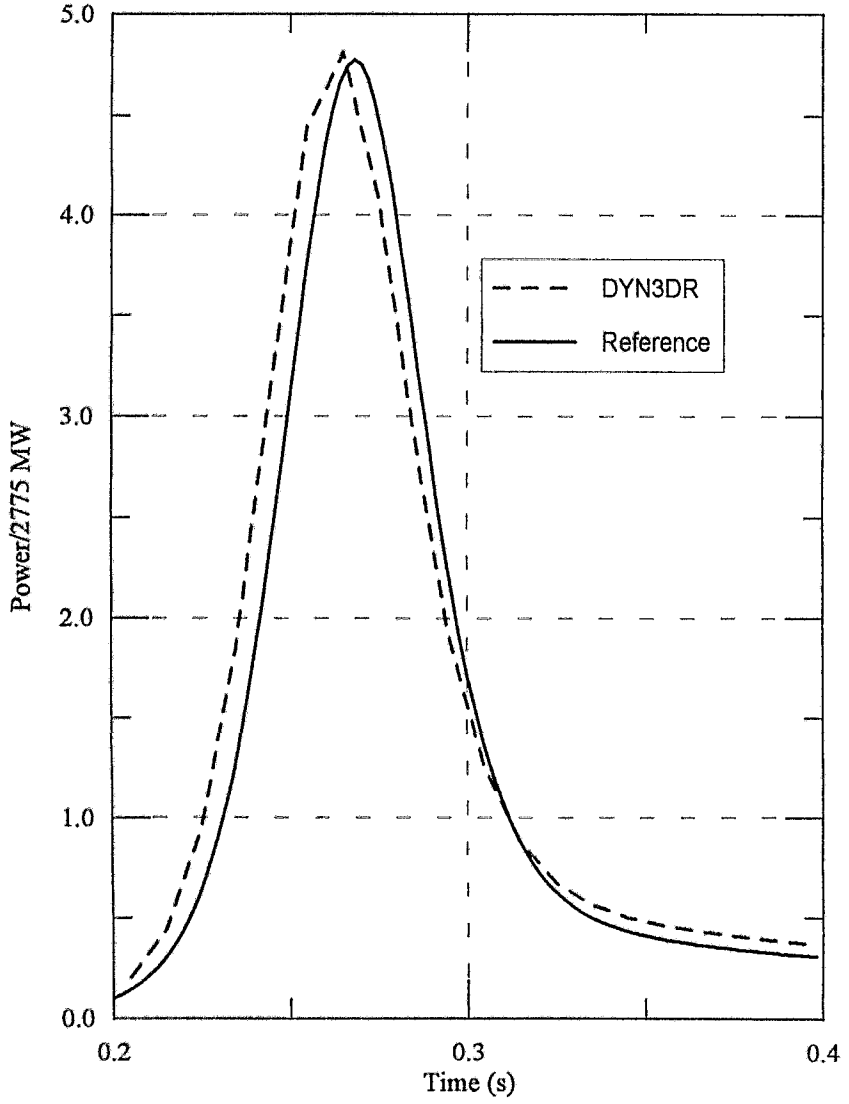


Fig. 3.C1.1: Nuclear Power

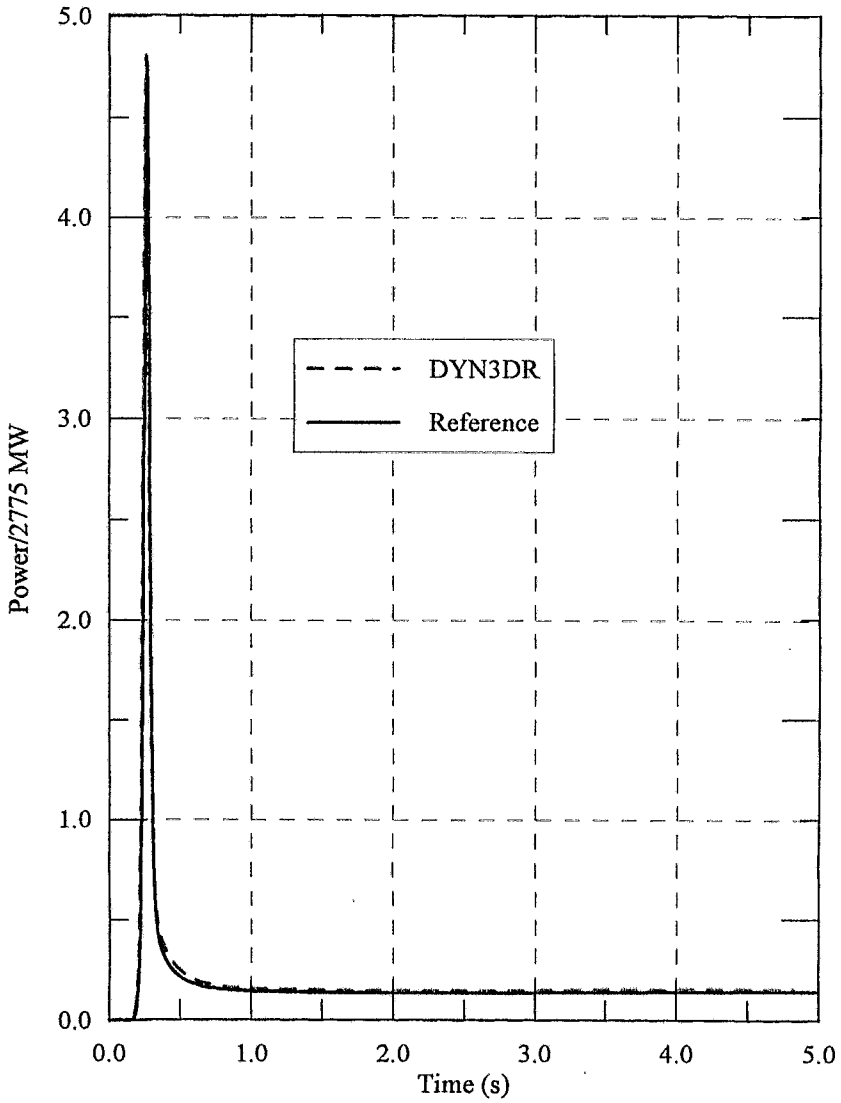


Fig. 3.C1.2: Nuclear Power

PWR Case C1: Ejection of a Peripheral Rod at HZP

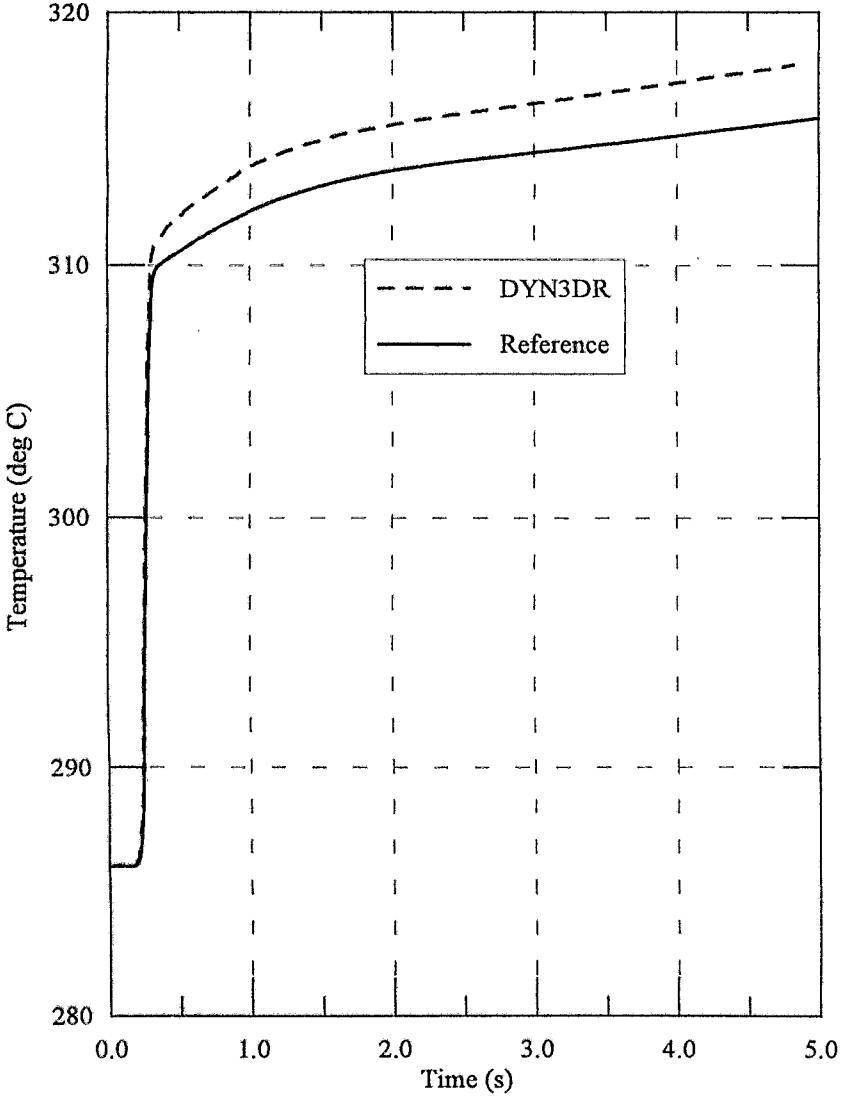


Fig. 3.C1.3: Core Averaged Doppler Temperature

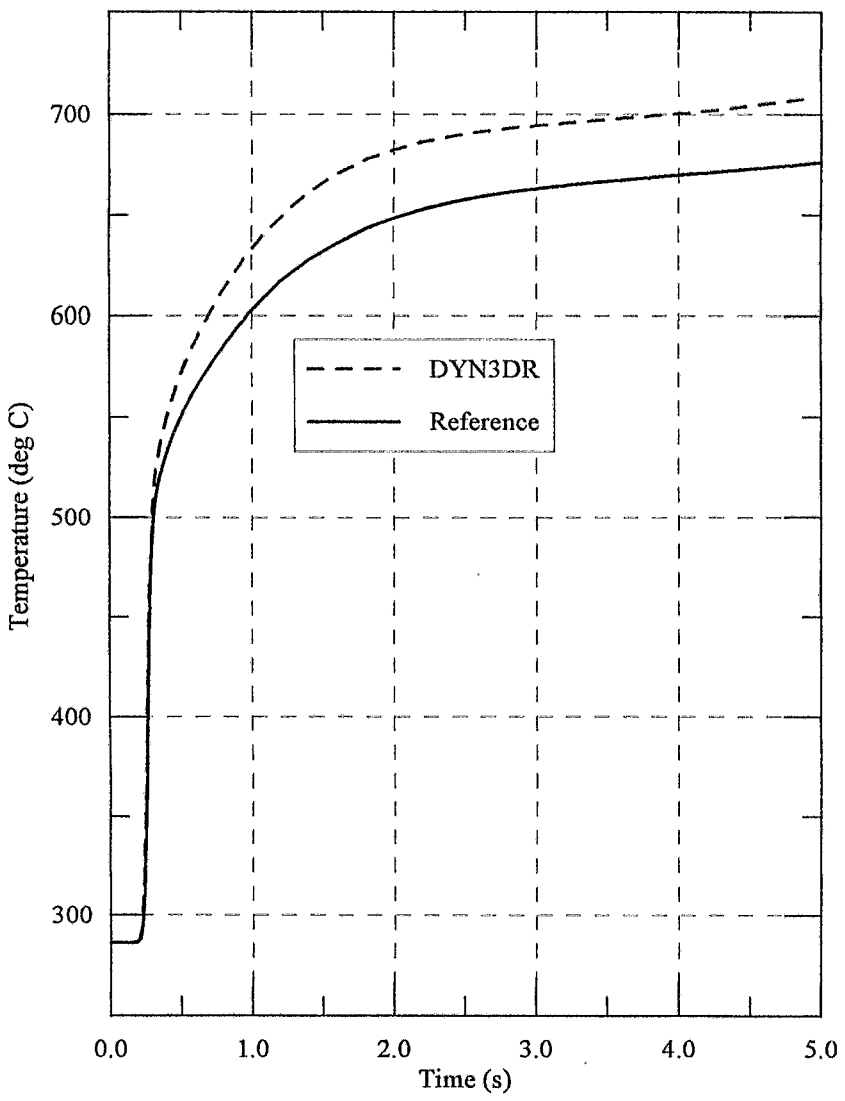


Fig. 3.C1.4: Maximum Fuel Centerline Temperature

PWR Case C1: Ejection of a Peripheral Rod at HZP

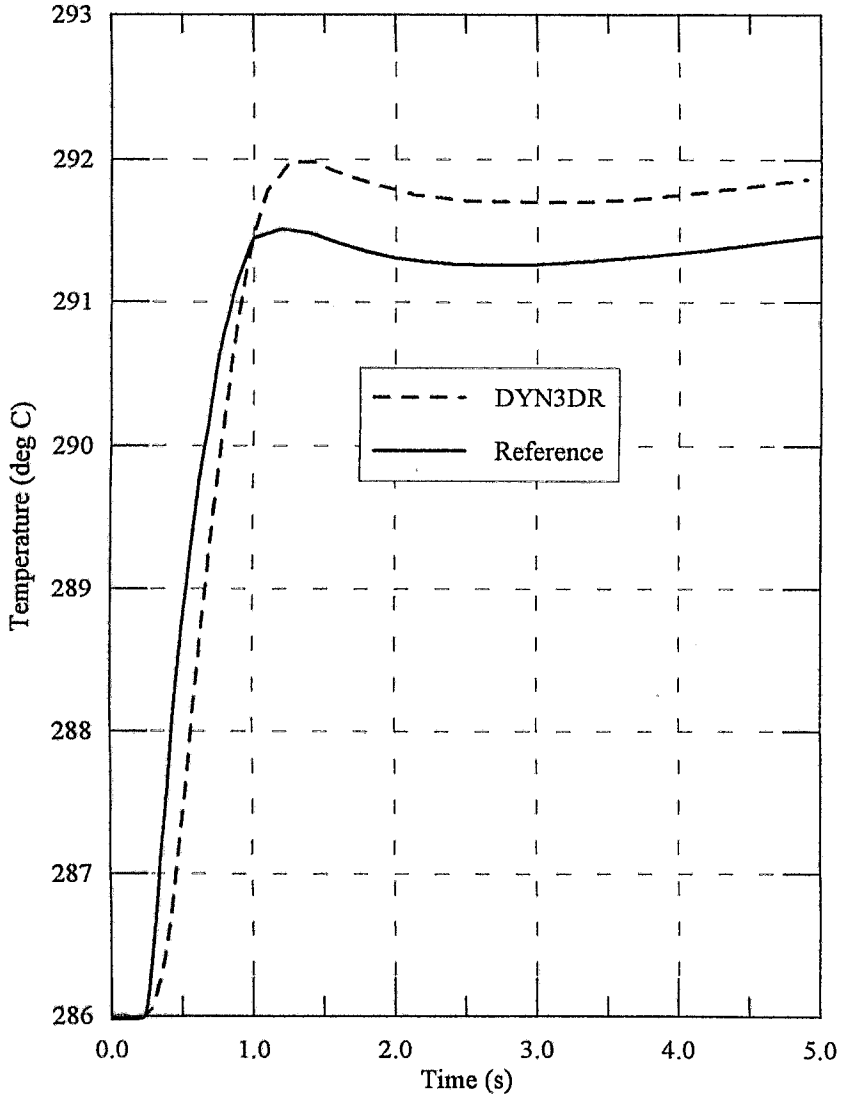


Fig. 3.C1.5: Coolant Exit Temperature

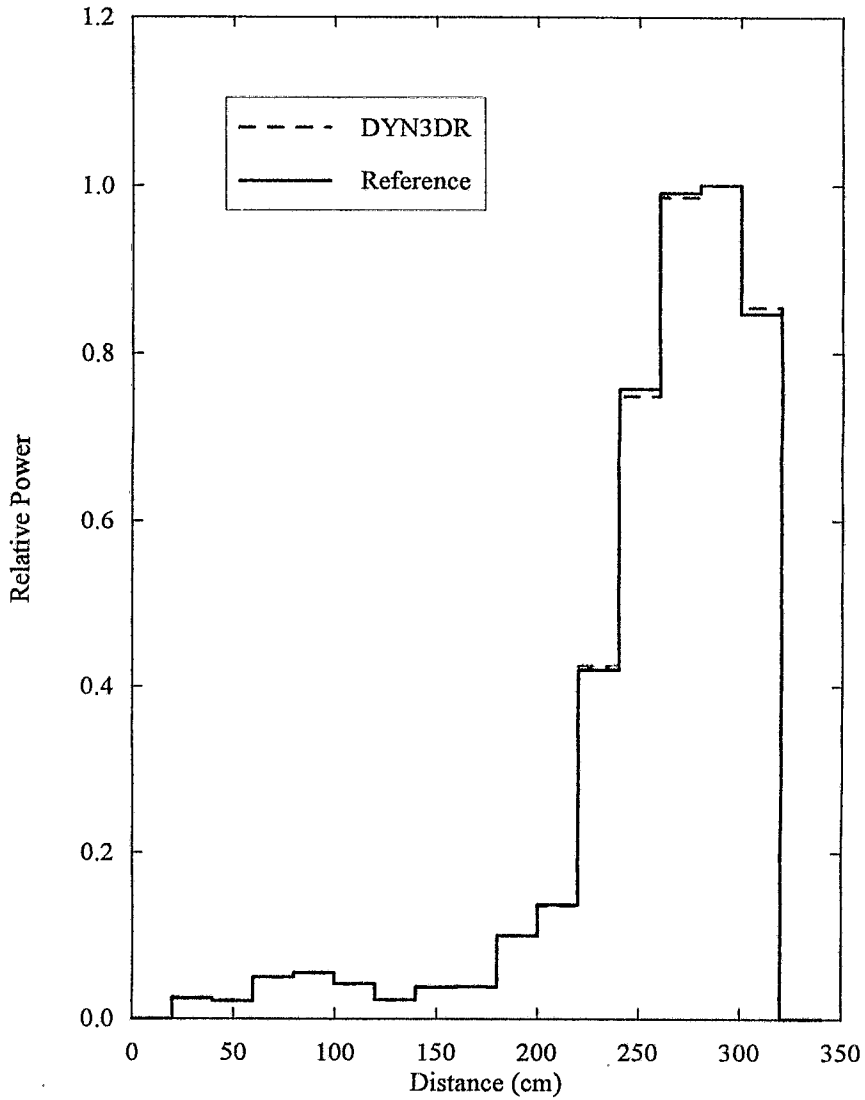


Fig. 3.C1.6: Radial Power Distribution at Time of Power Maximum in Axial Layer 13 (Along the Horizontal Traverse)

PWR Case C2: Ejection of a Peripheral Rod at FP

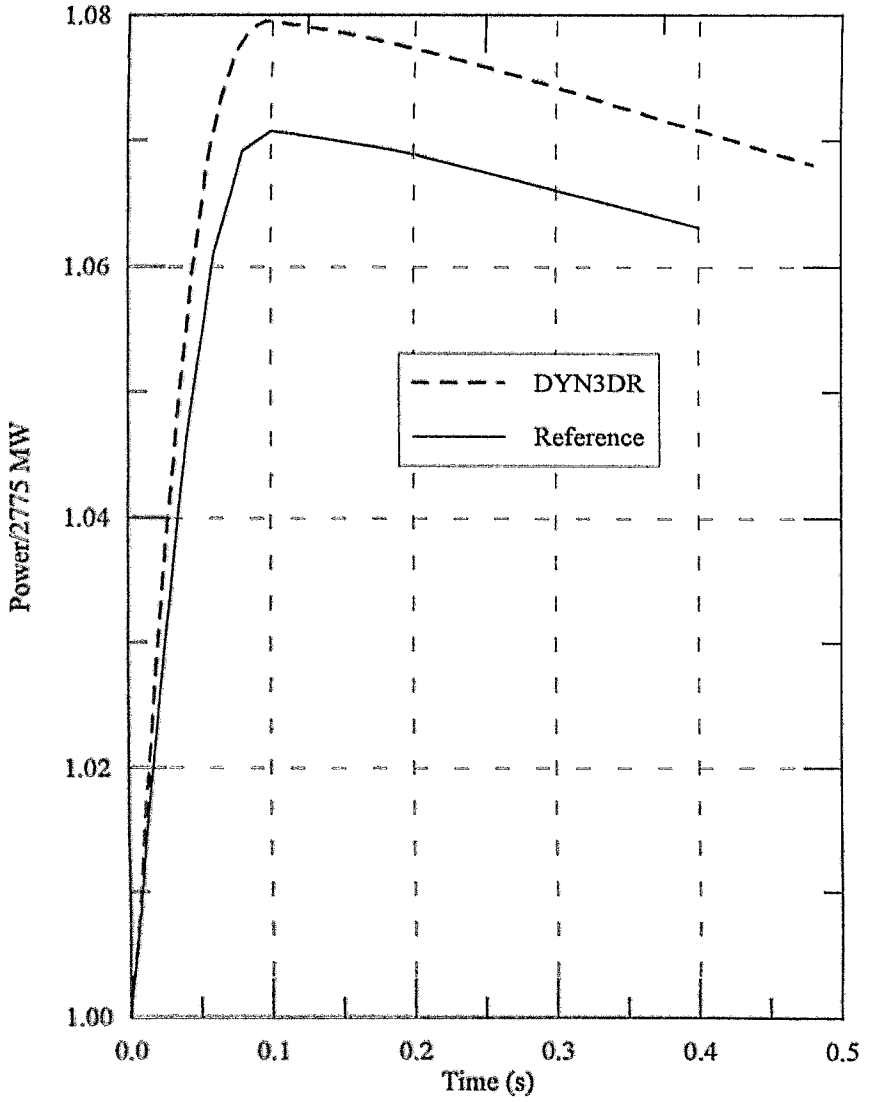


Fig. 3.C2.1: Nuclear Power

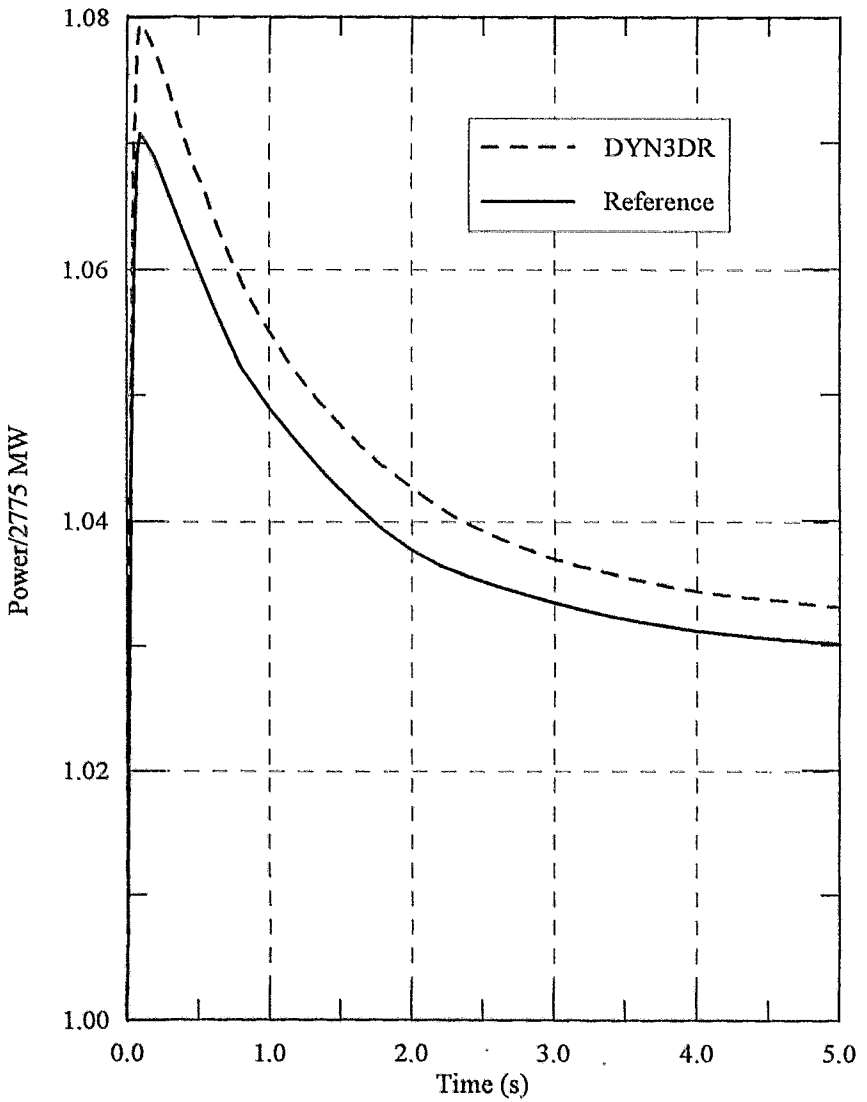


Fig. 3.C2.2: Nuclear Power

PWR Case C2: Ejection of a Peripheral Rod at FP

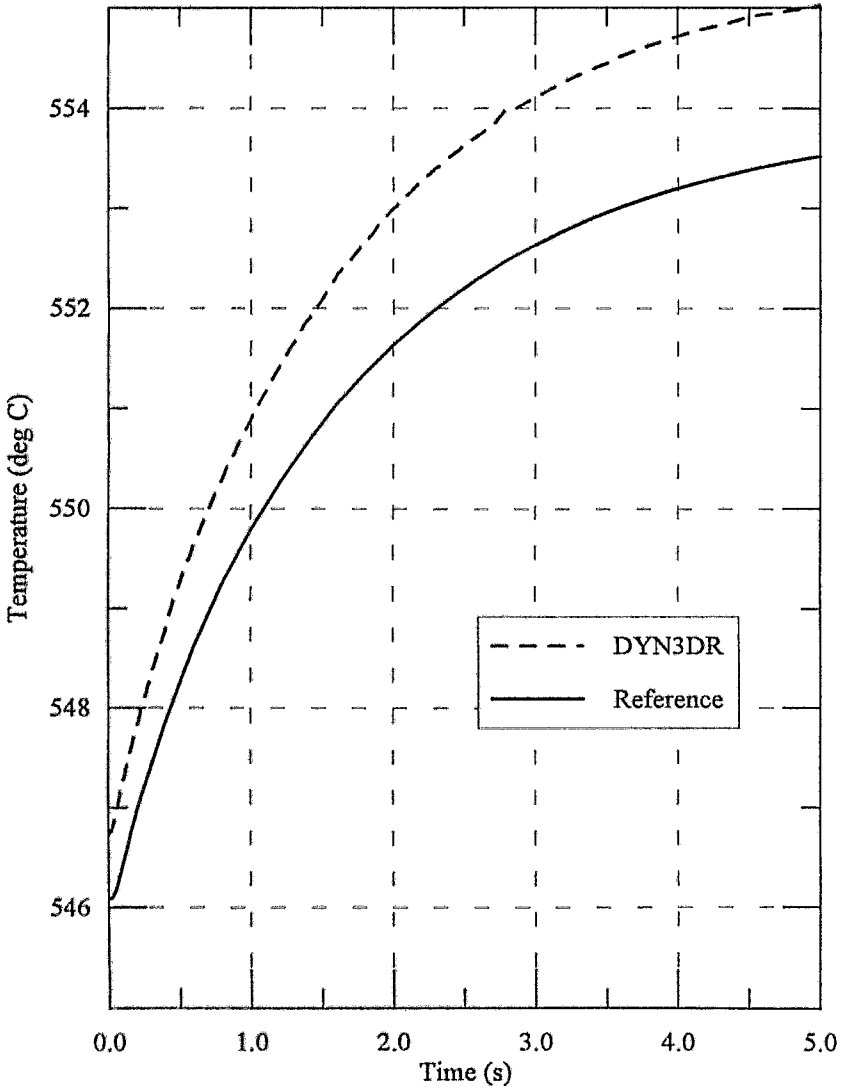


Fig. 3.C2.3: Core Averaged Doppler Temperature

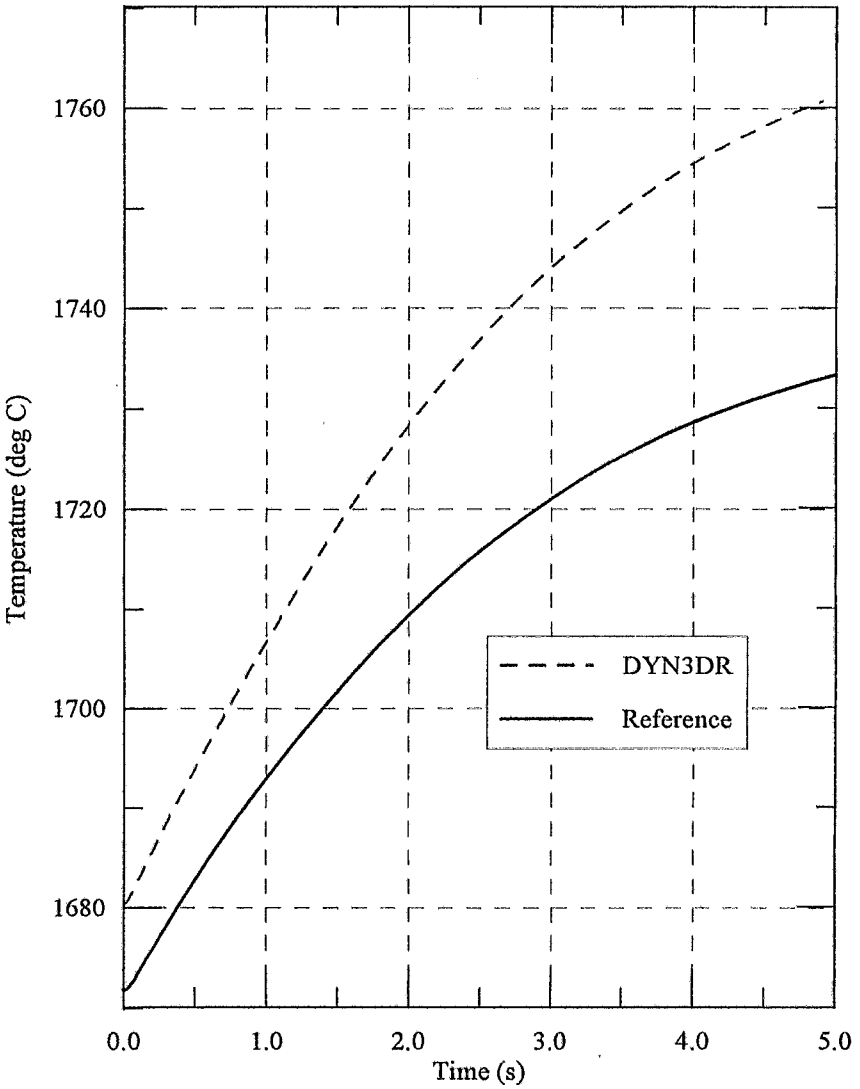


Fig. 3.C2.4: Maximum Fuel Centerline Temperature

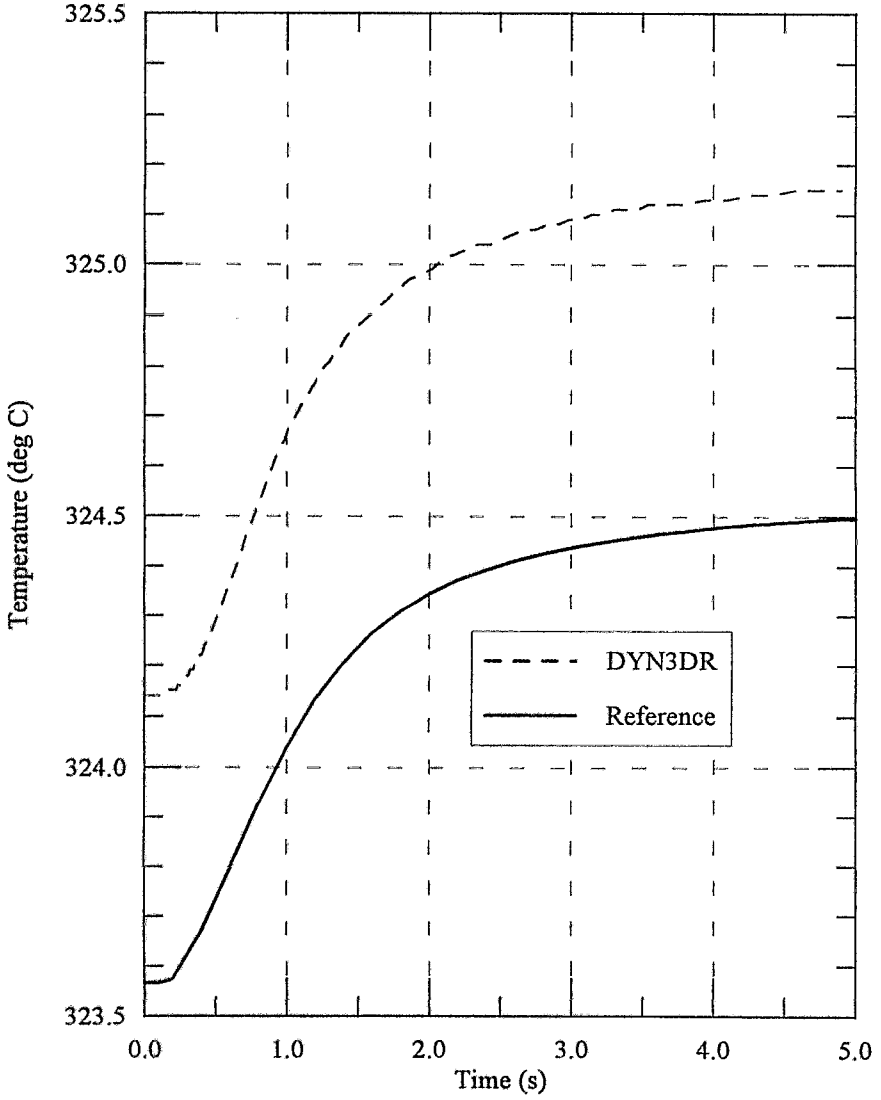


Fig. 3.C2.5: Coolant Exit Temperature

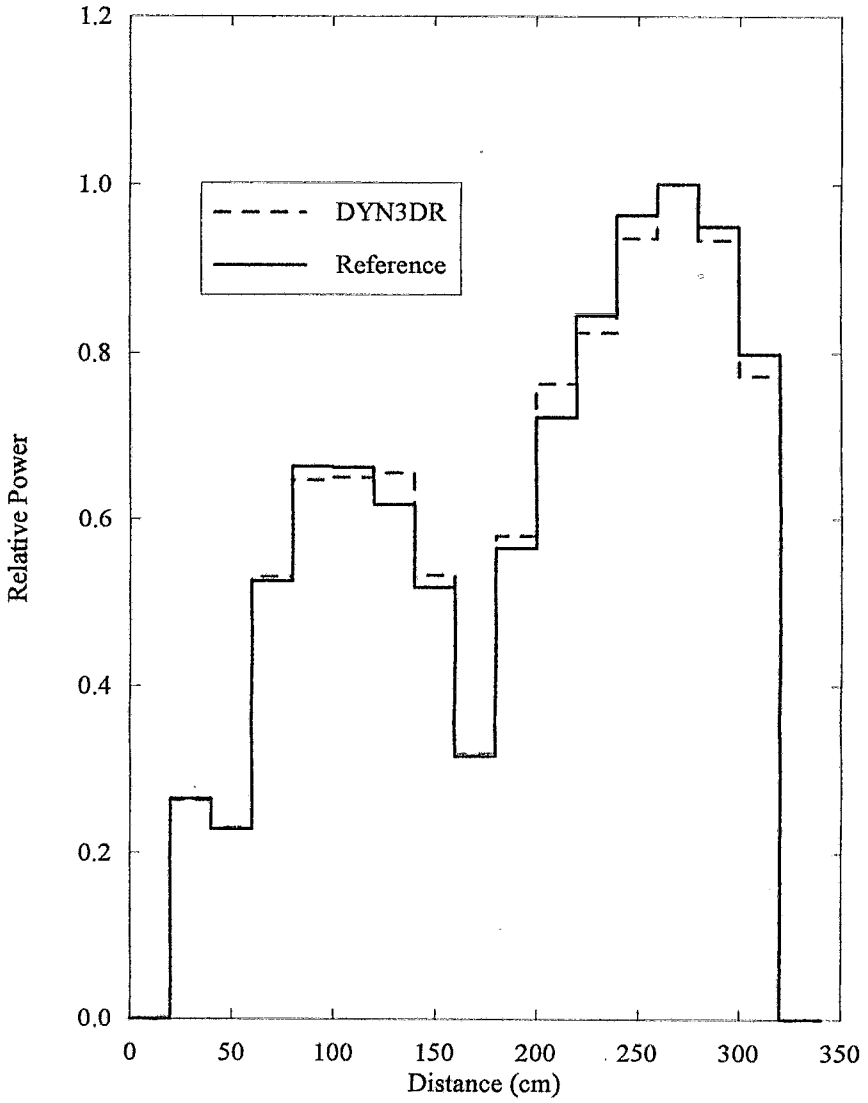


Fig. 3.C2.6: Radial Power Distribution at Time of Power Maximum in Axial Layer 13 (Along the Horozontal Traverse)

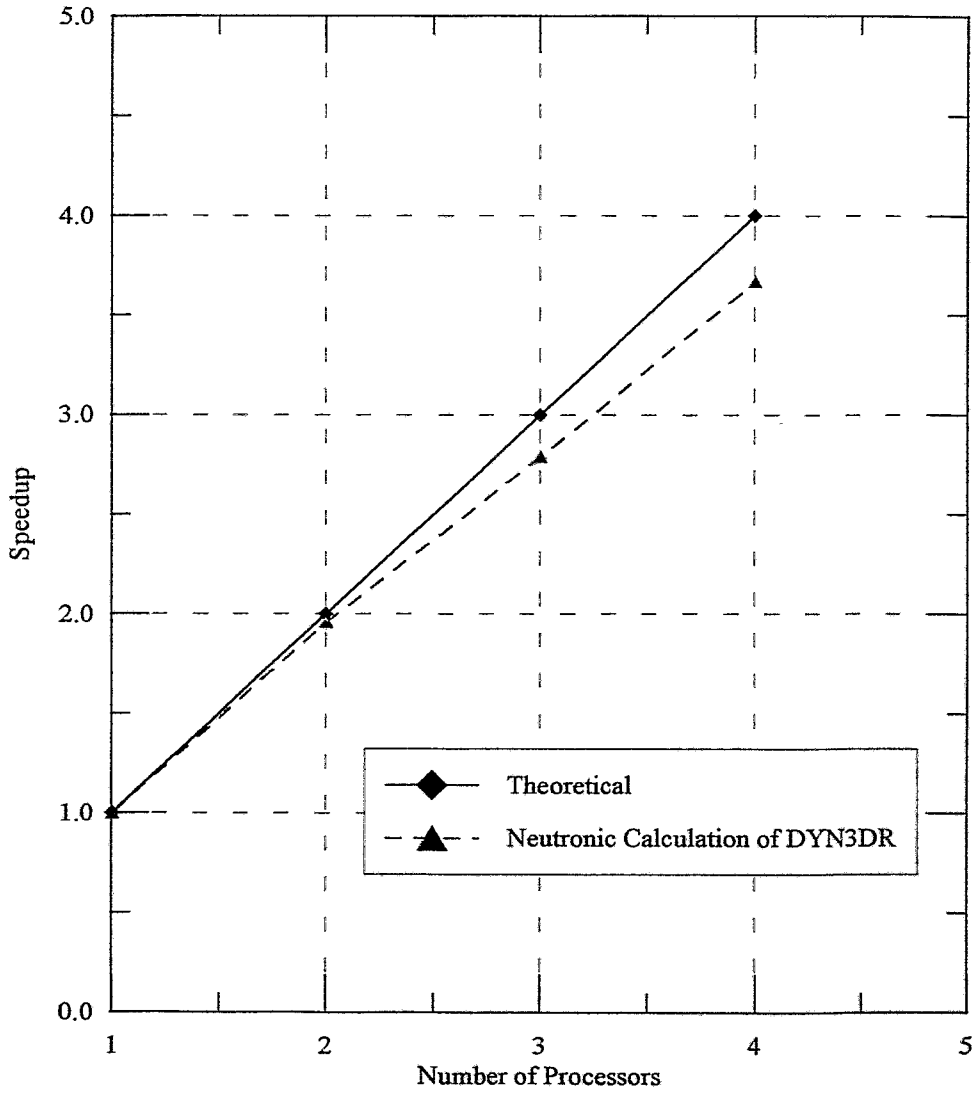


Fig. 4.1: Speedup of Steady State Neutronic Calculation in DYN3DR Using Different Number of Processors